Bioscience Reports (2021) **41** BSR20203424
https://doi.org/10.1042/BSR20203424

PORTLAND PRESS

Research Article

The model structure of the hammerhead ribozyme formed by RNAs of reciprocal chirality

Eliza Wyszko[1], Mariusz Popenda[1], Dorota Gudanis[1], Joanna Sarzyńska[1], Agnieszka Belter[1], Patrick Perrigue[2], Pawel Skowronek[3], Katarzyna Rolle[1] and Jan Barciszewski[1,2]

[1]Institute of Bioorganic Chemistry of the Polish Academy of Sciences, Noskowskiego 12, 61-704 Poznań, Poland; [2]NanoBiomedical Center of the Adam Mickiewicz University, Wszechnicy Piastowskiej 3, 61-614 Poznań, Poland; [3]Faculty of Chemistry of the Adam Mickiewicz University, Uniwersytetu Poznańskiego 8, 61-614 Poznań, Poland

Correspondence: Jan Barciszewski (Jan.Barciszewski@ibch.poznan.pl)

RNA-based tools are frequently used to modulate gene expression in living cells. However, the stability and effectiveness of such RNA-based tools is limited by cellular nuclease activity. One way to increase RNA's resistance to nucleases is to replace its D-ribose backbone with L-ribose isomers. This modification changes chirality of an entire RNA molecule to L-form giving it more chance of survival when introduced into cells. Recently, we have described the activity of left-handed hammerhead ribozyme (L-Rz, L-HH) that can specifically hydrolyse RNA with the opposite chirality at a predetermined location. To understand the structural background of the RNA specific cleavage in a heterochiral complex, we used circular dichroism (CD) and nuclear magnetic resonance (NMR) spectroscopy as well as performed molecular modelling and dynamics simulations of homo- and heterochiral RNA complexes. The active ribozyme-target heterochiral complex showed a mixed chirality as well as low field imino proton NMR signals. We modelled the 3D structures of the oligoribonucleotides with their ribozyme counterparts of reciprocal chirality. L- or D-ribozyme formed a stable, homochiral helix 2, and two short double heterochiral helixes 1 and 3 of D- or L-RNA strand thorough irregular Watson–Crick base pairs. The formation of the heterochiral complexes is supported by the result of simulation molecular dynamics. These new observations suggest that L-catalytic nucleic acids can be used as tools in translational biology and diagnostics.

Introduction

A fundamental feature of the proteins and nucleic acids is their homochirality. These natural biopolymers are composed of only one optically active 'isomer': L- amino acids or D-nucleotides. Although the origin of homochirality in biological macromolecules is not fully understood, it is assumed to be essential to ensure the high specificity and fidelity of the recognition mechanism between them. The stereospecificity of enzyme (protein) or ribozyme (nucleic acids) catalysed reactions is the foundation of the homochiral world.

Changing chirality is a strategy to overcome the low chemical stability of the phosphodiester bond of D-RNA in order to build more effective RNA-based tools. It is known that mirror-image ribonucleic acids consisting of L-ribose instead of D-ribose are resistant to hydrolysis with ribonucleases. Also L-DNA, where D-deoxyribose is substituted with L-deoxyribose, are resistant to nucleases [1,2]. Short interference RNAs (siRNAs) and catalytic RNAs (ribozymes) are widely used for modulation of gene expression [3], and it seems that a stable L-counterpart could be more suitable and attractive for their effectiveness in therapeutic applications [4]. It is generally accepted that the biggest advantage of nucleic acids for various applications is due to the propensity for complementary recognition of relevant nucleic acid strands by Watson–Crick base 'pairing': but these interactions require the substrate of the same chirality. This means that D-RNA or D-DNA can form base pairs with another D-RNA or D-DNA. However,

Received: 29 September 2020
Revised: 01 December 2020
Accepted: 22 December 2020

Accepted Manuscript online: 22 December 2020
Version of Record published: 08 January 2021

Bioscience Reports (2021) **41** BSR20203424
https://doi.org/10.1042/BSR20203424

30 years ago, L-DNA was proposed for use in antisense technologies, but stable duplexes of L/D-RNA with Watson–Crick base pairs have not been demonstrated [2,5,6]. Other studies have indicated that RNA heterochiral complexes are also not formed [7,8]. Similarly, 'L-oligonucleotides' composed of all four canonical nucleotides did not form a heterochiral helix with D-RNA or D-DNA [9]. On the other hand, heterochiral complexes between homopurine and homopyrimidine strands have been proposed, without the identification of an interaction mode between nucleic acid bases. Formation of non-canonical heterochiral pairs between L-$(dAp)_5$dA and D-poly(rU) have been suggested, but no hybridization of L-dU oligomer and D-poly(dA) was observed [10]. Also no complementarity has been detected between of L- and D-DNA with RNA containing all four base residues [9]. A few years ago it has been demonstrated that the mirror image RNA aptamer (L-RNA) binds to TAR RNA (D-RNA) and inhibits the formation of the TAR-tat complex critical to HIV-1 replication [11]. Recently, it has been shown *in vitro* that selected L-DNA aptamers bind to a D-RNA target [12], but Watson–Crick base pairs within that complex have been excluded [11,12].

The intense interest in enantiomeric nucleic acids observed in the last 40 years has dampened recently because the finding that L- and D- oligonucleotides do not form a regular double helix with Watson–Crick base pairs [13].

Recently, for the first time, some of us have shown that mirror image hammerhead ribozymes (L-ribozyme) and L-DNAzyme cleave the complementary D-RNA substrate of reciprocal chirality at the predetermined site [14,15]. On this basis, one can conclude that the enantiomeric nucleic acids could be used for regulation of their biological activity, and L-RNA could make valuable tools for potential therapeutic applications [15]. Here, we present new experimental results and extensive 3D molecular modelling data, that allow us to conclude that the interactions of the L-ribozyme with D-RNA target are possible. The results are based on the formation of irregular base-pairs with Watson–Crick type hydrogen bonding, that ensures the cleavage capacity and specificity of the L-ribozyme. The specific homo/heterochiral complex formation of the mixed chirality between D-substrate and L-ribozyme take place due to the strong homochiral structure of the central part of the ribozyme (helix 2), which induces and stabilizes conformational changes (χ, P angles and helical parameters) in the substrate strand, and facilitates its binding to the ribozyme. Our model also provides an explanation of why a complex of two linear complementary oligonucleotides with similar length, and reverse chirality cannot be formed.

Materials and methods

Oligonucleotides synthesis

Chemically synthesized RNA oligonucleotides were from IBA (Germany) or ChemGenes (U.S.A.). The 14-nt synthetic D- and L-RNA oligomers with the sequence 5′CUUCAAGUCCGCCA3′ were labelled with fluorescein at the 5′ end. The D-HH (D-Rz), L-HH (L-Rz) hammerhead ribozymes were 33-nt long with the sequence 5′UGGCGCUGA UGAGGCCGAAAGGCCGAAACUUGA3′. Nucleotides of L33 at positions 1-6 and 29-33 for parallel complex were methylated at 2′OH. D-anti HH Ribozyme 5′UGUCAGCUGAUGAGGCCGAAAGGCCGAACCAGCGG3′ was synthesized and labelled with FAM.

RNA hydrolysis with ribozymes *in vitro*

The activity of the D- and the L-hammerhead ribozymes with labelled L- and D-RNA targets were measured in 10 μl reaction volumes containing 50 mM Tris-HCl at pH 7.5 at 37°C. The RNA substrate and L- or D-Rz ribozymes were denatured for 2 min at 73°C and cooled to 25°C at a rate of 1°C/min. The reactions were done at 0 and 25 mM $MgCl_2$ concentrations. Hydrolysis products were separated with 20% polyacrylamide gel electrophoresis (PAGE) in the presence of 7 M urea in 0.09 M Tris-borate buffer at pH 8.3. The gels were exposed to a Fuji Film FLA 5100 phosphoimager using the manufacturer's (Fuji) BCIP/NBT Liquid Substrate System (Sigma), and bands were quantified using the ImageQuant software from Molecular Dynamics.

CD spectroscopy

CD spectra were recorded on a JASCO J-815 spectropolarimeter. The L- and D-oligonucleotides were dissolved in 50 mM NaCl, 20 mM Tris-HCl pH 7.5 buffer to achieve a concentration of 3.0 μM. All samples were denatured at 90°C for 5 min and then slowly cooled to room temperature before data collection [17]. The spectra were recorded in triplicate at 25°C in the 205–320 nm wavelength range with a 1 nm data interval. The buffer spectrum was subtracted from the sample spectra.

NMR spectroscopy

All NMR spectra were acquired on a Bruker AVANCE III 700 MHz spectrometer, equipped with a QCI CryoProbe. D-RNA, L-Rz and their equimolar amounts (3 μM) complex 3 were dissolved in buffer 150 mM NaCl, 50 mM

Tris-HCl pH 7.5 with 10 mM $MgCl_2$. Equimolar amounts D-RNA and L-Rz (L33) was dissolved in 150 mM NaCl and 10 mM sodium phosphate pH 6.8. The solvent was H_2O/D_2O (9:1, v/v). The samples were annealed by heating at 90°C for 5 min and then slowly cooled to room temperature. The 3 mm thin wall tubes were used with a final sample volume of 200 µl. The water signal was suppressed by excitation sculpting with a gradient pulse. Spectra were processed and prepared with TopSpin 3.2 Bruker Software.

Structure modelling and molecular simulations

The 3D structures of homochiral and heterochiral complexes of RNA hammerhead (Rz) ribozyme (33-mer) and RNA oligonucleotide (14-mer) were constructed based on the 3D crystal structure of the catalytic center of hammerhead ribozyme (3ZP8) with RNA Composer [16]. The 14 nt RNA substrate strand was joined to the ribozyme 3′-end through the GGG linker (17). This allowed building a model of the cis-acting ribozyme. RNA secondary structure predictions were performed through the Vienna RNAfold server (http://rna.tbi.univie.ac.at/cgi-bin/RNAfold.cgi). We incorporated the three-way junction motif covering the catalytic center of the ribozyme (PDB: 3ZP8). RNAfold generates up to ten structure models and we selected only the model with the lowest total energy. Visualizations of the molecular models were done in PyMOL (http://www.pymol.org). Finally, the linker was removed, and the structure was stored. The heterochiral model L/D we got from D/D structure with the X-Plor program ver. 2.21 [18]. The parameters for force field CHARMM (dna_rna_allatom.param) were extended with parameters for L-RNA nucleotides. Parameters for L-RNA differ from D-RNA only for the torsion angles nucleosides and impropers for that enforce ribose chirality. Parameters kchimpr differ only in the sign [18–21]. Furthermore, 1000 step minimalization was done using conjugate Powel Method, and restrained hydrogen bonds and planarity restrains for Watson–Crick base pairs.

Geometry of the D/D and D/L duplex models were of heterochiral complex. Correctness of the centre chirality was evaluated by a data processing validated with RCSB MAXIT (MAcromolecularEXchange Input Tool), covering geometry of covalent bond and chirality centres. The two other models L/L and L/D were obtained by changes of values of the Z axis from D/D and D/L, respectively.

The fours starting structures (models) of DL, LD, LL and DD were built using SYBYL and UCSF Chimera [21,22]. In the double-stranded segments, Watson–Crick base pairs were held with proper alignment and distance for each hydrogen bond. All these models was subjected to MD simulations.

MD simulations were performed with the AMBER18 package [23]. We used the *tleap* module of Amber 18 to prepare the topologies and coordinates for simulations. We utilized the AMBER ff99bsc0χ_{OL3} force field for D-RNA and its modified version for L-RNA [24,25]. The modification of ff99bsc0χ_{OL3} to account for L-ribonucleotides involved corrections of dihedral angles (γ and χ). Each of the structures was solvated with TIP3P water molecules in a truncated octahedral box with minimal distance of 10 Å between solute and the box border [26]. The systems were neutralized with Na^+ cations and NaCl excess salt was added to obtain the concentration of 150 mM by using Joung and Cheatham ion parameters [27]. The solvated systems were minimized and equilibrated. The minimization involved three series of 200 steps with steepest descent followed by 300 steps with the conjugate gradient method, first with position restraints of 25.5 kcal/mol Å^2 applied to solute atoms and finally without any restraints. Then, at the heating stage, the temperature was gradually raised to 300 K within 80 ps followed by 20 ps of equilibration while solute atoms restrained with harmonic potential of 15 kcal/(mol · Å^2). Next, the restraints were gradually released in four rounds (10, 5, 1 and 0.5 kcal/mol Å^2) of 100 ps each. After that, two sets of MD simulations were carried out: one set of entirely unrestrained simulations and a second set with small harmonic potential of 0.5 kcal/ mol · Å^2 applied to base heavy atoms of residues involved in Watson–Crick hydrogen bonding between heterochiral strands, to preserve these bonds and to allow the sugar-phospate backbone to adjust to it. The long-range electrostatics interactions were calculated using the particle mesh Ewald method, periodic boundary conditions, and the non-bonded cut-off set to 9 Å. The covalent bonds were constrained using SHAKE, and the integration time step was set to 2 fs. The Langevin thermostat with collision frequency 2.0 ps $^{-1}$ was used to control the temperature and the Berendsen barostat was used to enforce a constant pressure simulation. MD simulations were performed with the *pmemd* module of AMBER 18 on CUDA Device (Ge Force RTX2080). The data generated from MD were analysed using the CPPTRAJ module of Amber Tools [26].

Results

Recently, we have shown that L-hammerhead ribozyme (L-Rz, L-HH) hydrolysed a D-RNA target [15]. The chemically synthesized 33-nucleotide L-ribozyme (longer or bigger partner) cleaved the 14 nucleotides D-RNA substrate (shorter or smaller partner) at the predetermined location of GUC↓N (Figure 1). The model of mixed chirality be-

Bioscience Reports (2021) **41** BSR20203424
https://doi.org/10.1042/BSR20203424

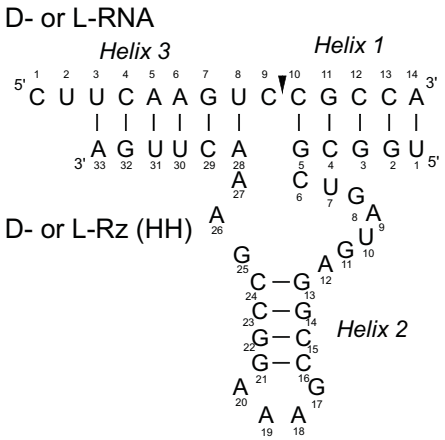

Figure 1. The secondary structural model of a L/D-hammerhead ribozyme (Rz) complexed with an L/D-RNA substrate containing GUC↓N, the predetermined cleavage site for hammerhead ribozymes

The arrow identifies specific cleavage site for all ribozymes. Each heterochiral catalytic complex contains the classical Watson–Crick homochiral base pairs forming stem core of ribozyme helix 2, (stem 2), which induce and stabilize heterochiral Watson–Crick like base pairs with substrate helices 1 and 3.

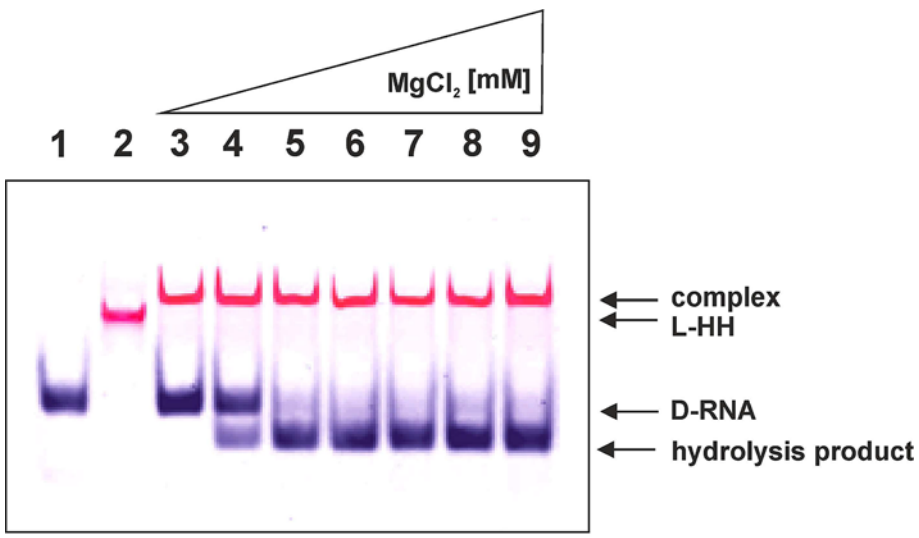

Figure 2. Visualization of intermediates and D-RNA hydrolysis with L-hammerhead ribozyme (L-HH)

D-RNA substrate of 14 nucleotide long (0.25 μM) labelled with FAM was incubated with 2.5 μM L-HH ribozyme labelled with cy5 and 4 μM cold L-HH at 70°C during 2 min, then mixture was fast cooled down, then reaction was incubated during 3h at 37°C in presence of increasing concentration of $MgCl_2$ (0.5, 1, 5, 10, 15, 20, 25 mM, lanes 3, 4, 5, 6, 7, 8, 9, respectively) in binding buffer (50 mM Tris-HCl pH 7.5, 160 mM KCl, 10 mM spermidine). Analysis was done on 15% native polyacrylamide gel with 2.5% glycerol. Lane: 1- D-RNA; 2 – L-HH ribozyme.

tween L-hammerhead ribozyme with D-RNA substrate is based on nucleotide sequence complementarity. Two short heterochiral helixes (helices 1 and 3) are formed between flanking parts of L-ribozyme with the substrate, but helix 2 of the catalytic L-RNA is always homochiral and stable.

To understand a mechanism of the active complex formation between D-RNA substrate and L-RNA ribozyme, we checked its migration on a native polyacrylamide gel. Using specifically colour-labelled reagents, we were able to show that D-RNA substrate forms the complex with L-ribozyme (L-HH) and migrates slowly (Figure 2). One can see, that in the presence of magnesium and 20 fold excess, L-hammerhead (HH) ribozyme specifically cleaved D-RNA target [15], and the expected hydrolysis products were observed (Figure 2). This observation was confirmed with results on

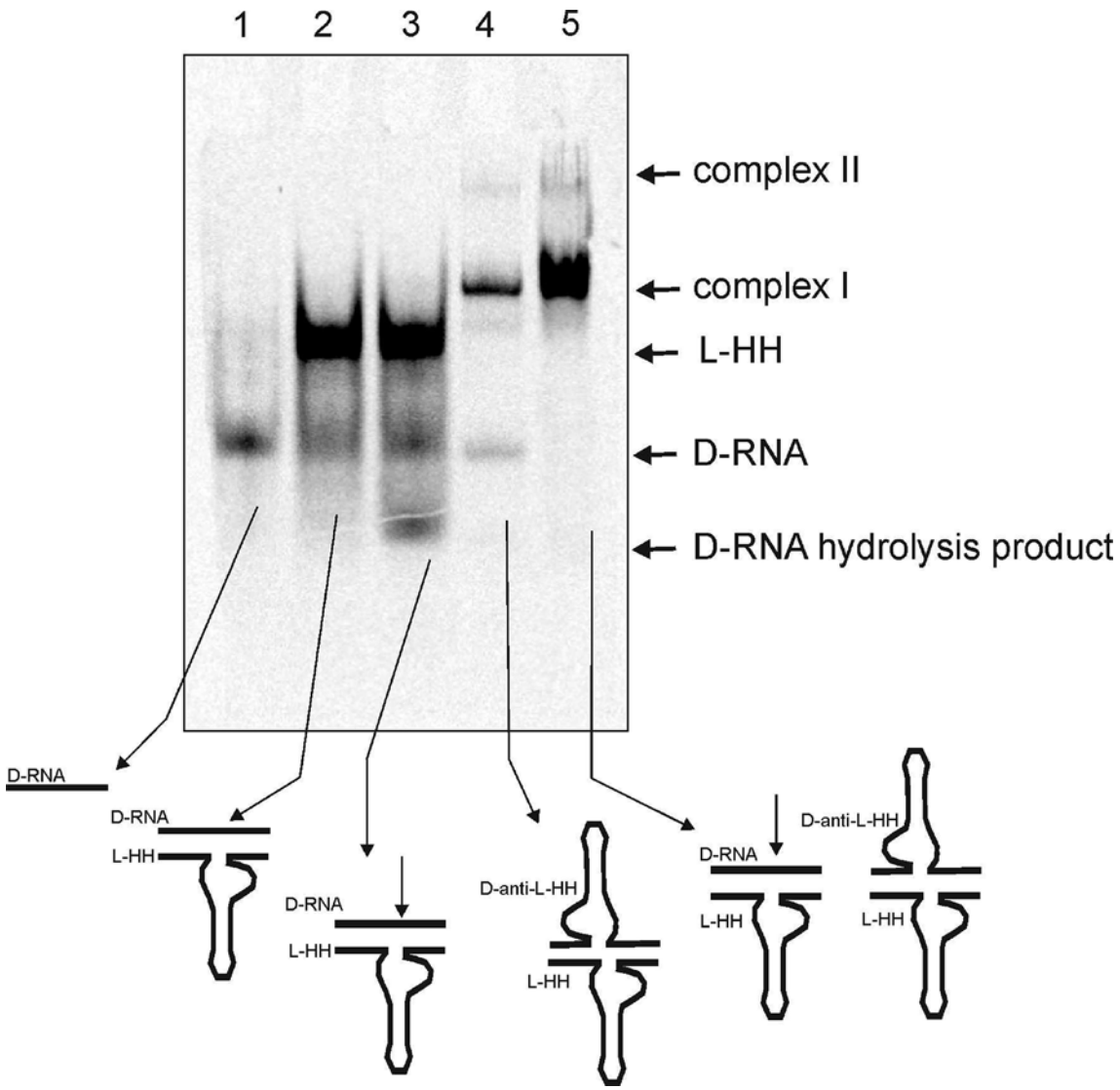

Figure 3. Analysis of complex formation of heterochiral RNAs

1. D-RNA target incubated in binding buffer containing 25 mM $MgCl_2$ (see Figure 2), 2. D-RNA target incubated in binding buffer with L-HH ribozyme, 3. D-RNA and L-HH ribozyme incubated in binding buffer containing 25 mM $MgCl_2$, 4. D-RNA, L-Rz ribozyme and anti D-Rz ribozyme in binding buffer, 5. D-RNA, L-Rz ribozyme and anti D-Rz ribozyme incubated in binding buffer containing 25 mM $MgCl_2$. Arrows shows cleavage products and complex formation position.

Figure 3. One should notice that specific hydrolysis takes place in the presence of magnesium ions (Figure 3, Lane 3). Interestingly, no specific cleavage was observed when L-HH ribozyme was complexed with D-anti-HH-ribozyme even in the presence of $MgCl_2$ (Figure 3). One should notice that both molecules have the strong secondary structure, particularly helix 2 and the same size.

To get a deeper insight into the conformation of the heterochiral complexes, we measured the CD spectra of L/D-ribozymes with L/D-RNA substrates (Figure 4). The L- or D-ribozymes are characterized by negative or positive CD band at 263 nm, respectively. The CD spectra of the homochiral structures for left-handed L-RNA and right-handed D-RNA substrates adopt negative or positive Cotton effect, respectively. That CD plot for L-HH is a mirror image of the CD plot obtained for the structure of the D-hammerhead ribozyme (D-HH). For the heterochiral complex of a ribozyme with RNA substrate, a difference between the Cotton effect of the renatured complex, the mixture of the ribozyme, and the substrate and their mathematical sum was detected (Figure 4A,B). The observed

Bioscience Reports (2021) **41** BSR20203424
https://doi.org/10.1042/BSR20203424

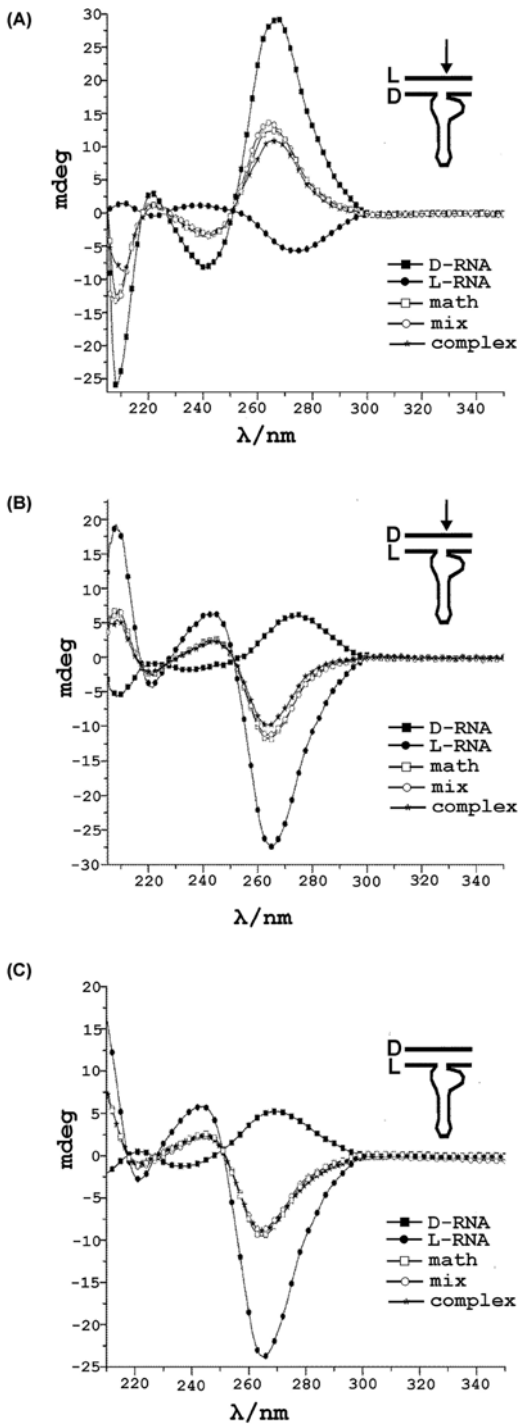

Figure 4. Circular dichroism (CD) spectra of heterochiral complexes of L- and D-hammerhead ribozyme with D- or L-RNA targets in 20 mM Tris pH 7.5 and 50 mM NaCl at room temperature

CD spectra are plotted as ellipticity (millidegrees) versus wavelength. Smooth curves represent the average of three separated scans at 1 nm sampling interval from 210 to 350 nm. (**A**) CD spectra of L-RNA target in complex with D-RNA (hammerhead ribozyme). (**B**) D-RNA target with L-RNA (hammerhead ribozyme). (**C**) control experiment with the use of D-RNA (5′GGCGACCGACUGU3′) not fully complementary to L-RNA (hammerhead ribozyme). There are differences in the Cotton effect of the complexes. Black squares correspond to D- or L-RNA (ribozyme), (33-mer); black circles refer to L- or D-RNA target (14-mer), open squares represent mathematical sum of CD spectra of hammerhead ribozyme and RNA target, open circles correspond to a mixture of D-or L-hammerhead ribozyme with D-or L-RNA target without incubation step. Black stars show a complex of D- or L-RNA (ribozyme) with D- or L-RNA target preincubated at 90°C and slowly renatured overnight.

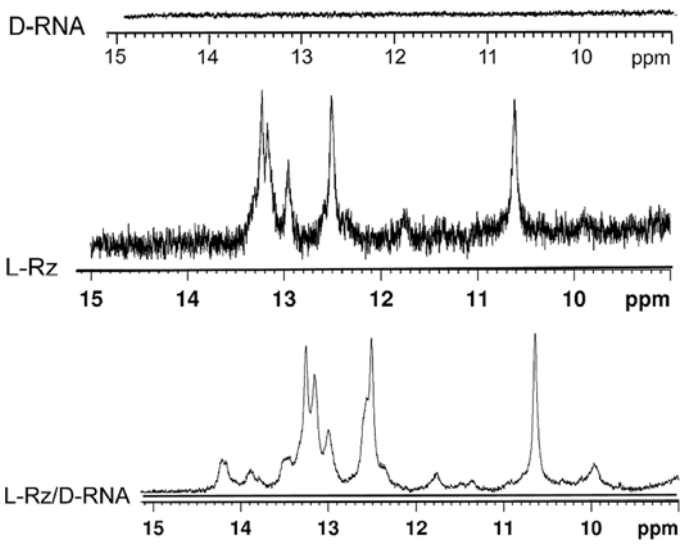

Figure 5. The imino region of ^{1}H NMR spectra of: D-RNA target, L-Rz ribozyme alone and D-RNA/L-Rz complex with 150 mM sodium chloride, 10 mM Tris-HCl buffer and 0.1 mM EDTA at 25°C

final Cotton effect for heterochiral complexes is reduced in comparison to the sum of individual components and the mixture of these components.

Figure 4A shows a right-handed complex because of the presence of D-RNA, for example, D-hammerhead ribozyme and Figure 4B presents a left-handed complex due to L-RNA, for example, L-hammerhead ribozyme. The important contribution of the sequence complementarity between ribozyme and the target for heterochiral complex formation was seen on Figure 4C. The lack of specific base pairing (Watson–Crick base pairs) between the target D-RNA and the L-RNA (hammerhead ribozyme) did not lead to the complex formation and therefore specific hydrolysis was excluded (Figure 4C).

To confirm the formation of heterochiral complexes and evaluate the nature of hydrogen bonding interactions in these complexes, we recorded the ^{1}H NMR spectra. They show spectra of single-stranded D-RNA or L-RNA (Figure 4) without imino proton signals. This indicated the lack of intrinsic secondary structure for the substrate strands. In contrast, several imino proton signals in the 10-14 ppm region were observed for the L-ribozyme, in general, in agreement with their secondary structures predicted by the RNA structure software [21,22]. For the heterochiral complex D-RNA/L-Rz, new imino-proton signals appeared in the range of 13.5-14.5 ppm (Figure 5). This is clearly demonstrated by the formation of Watson–Crick hydrogen bonds which stabilize the complex. To confirm the specific complex formation, we recordered ^{1}H NMR spectrum of putative heterochiral complex of L-Rz/D-RNA designed in such a way that helices 1 and 3 should form the parallel duplex (Supplementary Figure S1). For the complex with parallel stems new imino-proton signals in the region of 13–14.5 ppm were also observed: however, their pattern and intensity were different than those obtained for anti-parallel heterochiral catalytic complex (Supplementary Figure S2). It suggests that the nature of the hydrogen bond interactions is different for the parallel and anti-parallel complex.

Having experimental data on the specific hydrolysis of RNA with catalytic nucleic acids (zymes) in a heterochiral manner [15] as well as biophysical data (this paper), we calculated the 3D structures of the active heterochiral complexes. Because of the experimentally observed high specificity of D-RNA cleavage, it is obvious that the L-catalytic nucleic acids and the D-RNA substrate form a double strand with Watson–Crick hydrogen bonding network. It is required for the formation of the active site of ribozyme and the specific cleavage of the substrate at the GUC target [28,29].

To understand how this complex is self-assembled, we developed a new approach to find the possible configuration of L-nucleosides. We started with the right-handed homochiral complex of D-RNA/D-ribozyme, called the D/D RNA model (Figure 6A). The model of the 3D structure of homochiral right-handed complex of D-RNA target with D-Rz (ribozyme) was calculated on the basis of the crystallographic data (3ZP8) using an automated 3D structure modelling algorithm, Composer, invented by one of us [16]. The secondary structure of the hammerhead ribozyme input data was the same as in [17]. The D/D RNA model was transformed into heterochiral complex L-RNA/D-Rz (Figure 6A) by energy minimization with the Charm Field Force [19–21] using X-plor programme [18].

Bioscience Reports (2021) **41** BSR20203424
https://doi.org/10.1042/BSR20203424

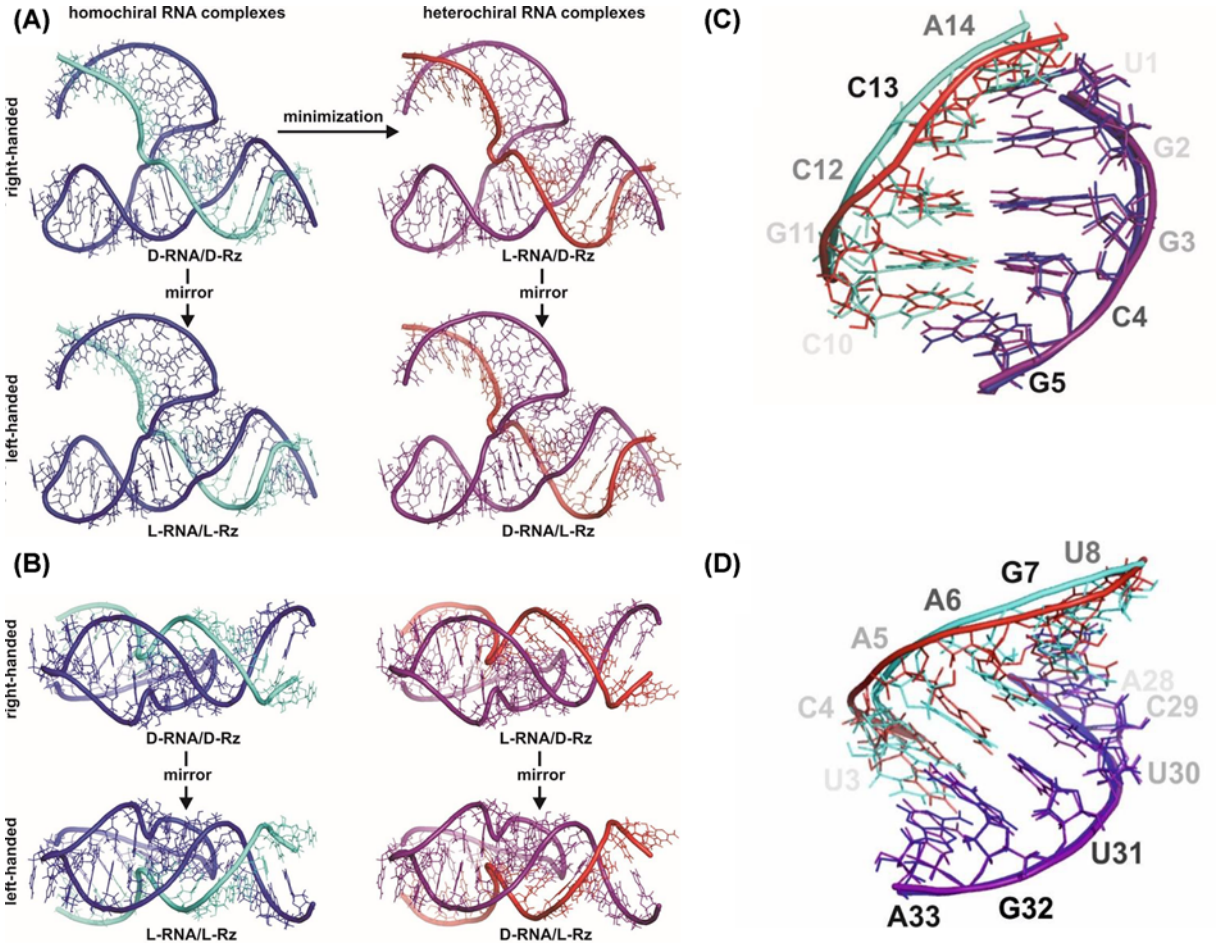

Figure 6. The 3D structure model of homochiral and heterochiral complexes of RNA hammerhead (Rz) ribozyme (34-mer) with RNA oligonucleotide (14-mer) as well as their fragments, modeled with Composer [18] and X-plor [19], respectively

(**A**) Transformation of right handed homochiral to heterochiral RNA complex by energy minimalization. Left handed complexes were obtained by mirror image. (**B**) Perpendicular view of four RNA complexes generated in A: D-RNA/D-Rz; L-RNA/D-Rz; L-RNA/L-Rz and D-RNA/L-Rz. (**C**) Overlapping of the 5′ end of D-hammerhead ribozyme in complex with D- RNA or L-RNA targets. The pentanucleotide $C_{10}GCCA_{14}$ sequence of D-RNA (green) or L-RNA target (red) at the 3′end forms Watson–Crick base pairs with U_1GGCG_5 residues at the 5′ end of D-RNA hammerhead ribozyme. (**D**) Overlapping of the 3′ end of D-hammerhead ribozyme in complex with 5′ end of D- RNA (green) or L-RNA (red) target. Watson–Crick interactions between U_3CAAGU_8 of D- or L-RNA target sequence at the 5′end with hexanucleotide of $A_{28}CUUGA_{33}$ at the 3′ end of D-RNA hammerhead ribozyme are visible.

The parameters of the complex, such as the bond lengths, angles between covalent bonds, electrostatic charges, and Van den Waals radii were the same for L-nucleotides and for their D enancjomers [21,22], except for the chiral centers and torsial angles, which have the opposite sign. These parameters allow a configuration change from D-RNA to L-RNA during energy minimalization (Figure 6A). The complexes of homochiral L-RNA/L-Rz complex and heterochiral D-RNA/L-Rz complex were obtained by mirror operations (Figure 6A,B). The sign of the atomic *Z*-coordinates of the right-handed (D-RNA/D-Rz) homochiral complex multiplied by -1 leads into the left-handed homochiral L-RNA/L-Rz complex (Figure 6A). The mirror image of L-RNA/D-Rz leads to D-RNA/L-Rz (Figure 6A,B).

Comparison of both the overall homochiral model complexes L/L and D/D (Figure 6) for heavy atoms (1000 atoms) showed Root Mean Square Deviation (RMSD) of 10.038 Å, but the RMSD for the RNA substrate and ribozyme were 5.520 Å (289 atoms) and 9.321 Å (711 atoms), respectively. On the other hand, a comparison of the heterochiral complex L/D with its homochiral counterpart D/D carried out with the Composer, showed a RMSD of 0.894 Å. Interestingly, the RMSD for a D substrate (289 atoms) was 1.484 Å, but it was 0.446 Å for L-ribozyme (711 atoms).

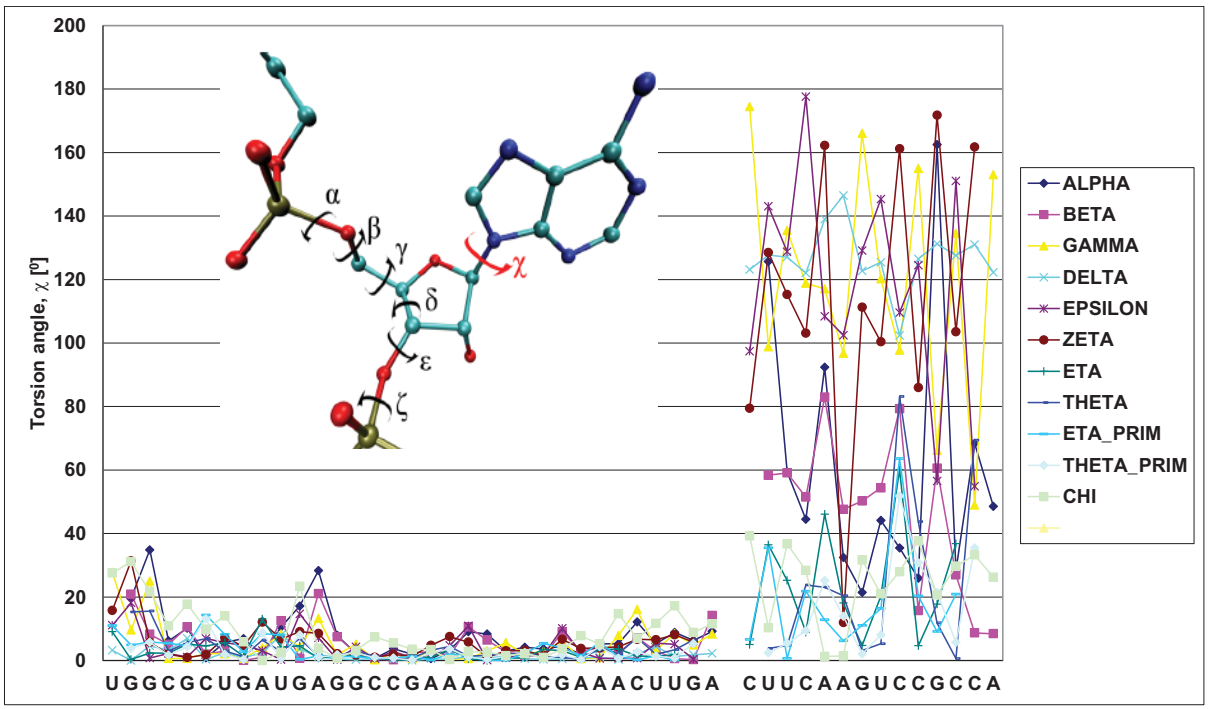

Figure 7. Differences of values of angles for all nucleotides in D- and L- hammerhead ribozyme and D and L-RNA target oligonucleotides

Different views of all four model complexes showed their structural similarities (Figure 6A,B). The most important part of the heterochiral complex models were interactions between RNAs of reverse chirality, for example, the double helixes 1 and 3 [H1, H3]. For H3 U_3CAAGU_8 of D- or L-target and $A_{28}CUUGA_{33}$ of D- or L-Rz (HH), one can clearly see that Watson-Crick type base pairs within the heterochiral complex were very similar to those of the homochiral complex with some irregularities (Figure 6D). RMSD for the heptanucleotide heterochiral duplex of 383 atoms is 1.279 Å. Detailed comparison of parts of the target RNA and the ribozyme showed RMSD of 0.950 and 0.408 Å, respectively. The same concerns the helix 1 (H1) of the other end of the complex (Figure 6C). The RMSD of heterochiral double helix of residues 10–14 of target RNA with residues of 1–5 of the ribozyme is 1.438 Å (for 322 atoms), but RMSD of each part of the complex target RNA and the ribozyme, is 1.014 and 0.617 Å, respectively. The small alterations observed in nucleoside conformation of the double-stranded RNA (Figure 6C,D) are due to the variations in the backbond angles (Figure 7). To get insight on the structure of the heterochiral complex, we analysed differences in values of all angles characteristic for a nucleotide conformation (Figure 7 and Supplementary Figures S3–6). One can see only minor variations in the angles of the L-hammerhead ribozyme structure (Figure 7, left sequence). On the other hand, differences in the structure of the target D-RNA model are larger (Figure 7, right sequence). The values of Chi orientation of base about glycosidic bond (Chi angle) values in heterochiral complex model differ, although all nucleosides exist in anti conformation (Figures 7 and 8A). One should also notice that the phase angle of the pseudorotation (P) values are similar in the homochiral complex (Figure 8B,C) and nucleoside 9 (cleavage site) shows the S conformation (C2′endo) [30–32]. In the heterochiral complex, this nucleotide occurs in the N conformation (C3′endo) (Figure 8B). A summary of pseudo rotation (P) and Chi angles changes (Figure 9) clearly showed the full symmetry between D-Rz/D-RNA and L-Rz/L-RNA homochiral, as well as D-Rz/L-RNA and L-Rz/D-RNA heterochiral complex models. In the next step, we calculated RMSD of ribose-phosphate backbone to evaluate the stability of two homochiral D/D and L/L (Supplementary Figure S7) and heterochiral D/L and L/D complexes without any restrictions (free) (Supplementary Figure S8). The RMSD for whole homochiral complexes show small fluctuations; formation of the D/D and L/L homochiral complexes is effected by classical Watson-Crick base pairs. The same concerned the active centre and all three helices. From analysis of the heterochiral D/L and L/D complexes one can see similar trajectories for helix (stem) 2 that is actually homochiral, and helixes (stems) 1 and 3 that are heterochiral. The last ones can be formed by slightly modified Watson–Crick base pairing. Trajectories for the complexes with constraints on the heavy atoms seem to be similar (Supplementary Figure S9). The observed changes

Bioscience Reports (2021) **41** BSR20203424
https://doi.org/10.1042/BSR20203424

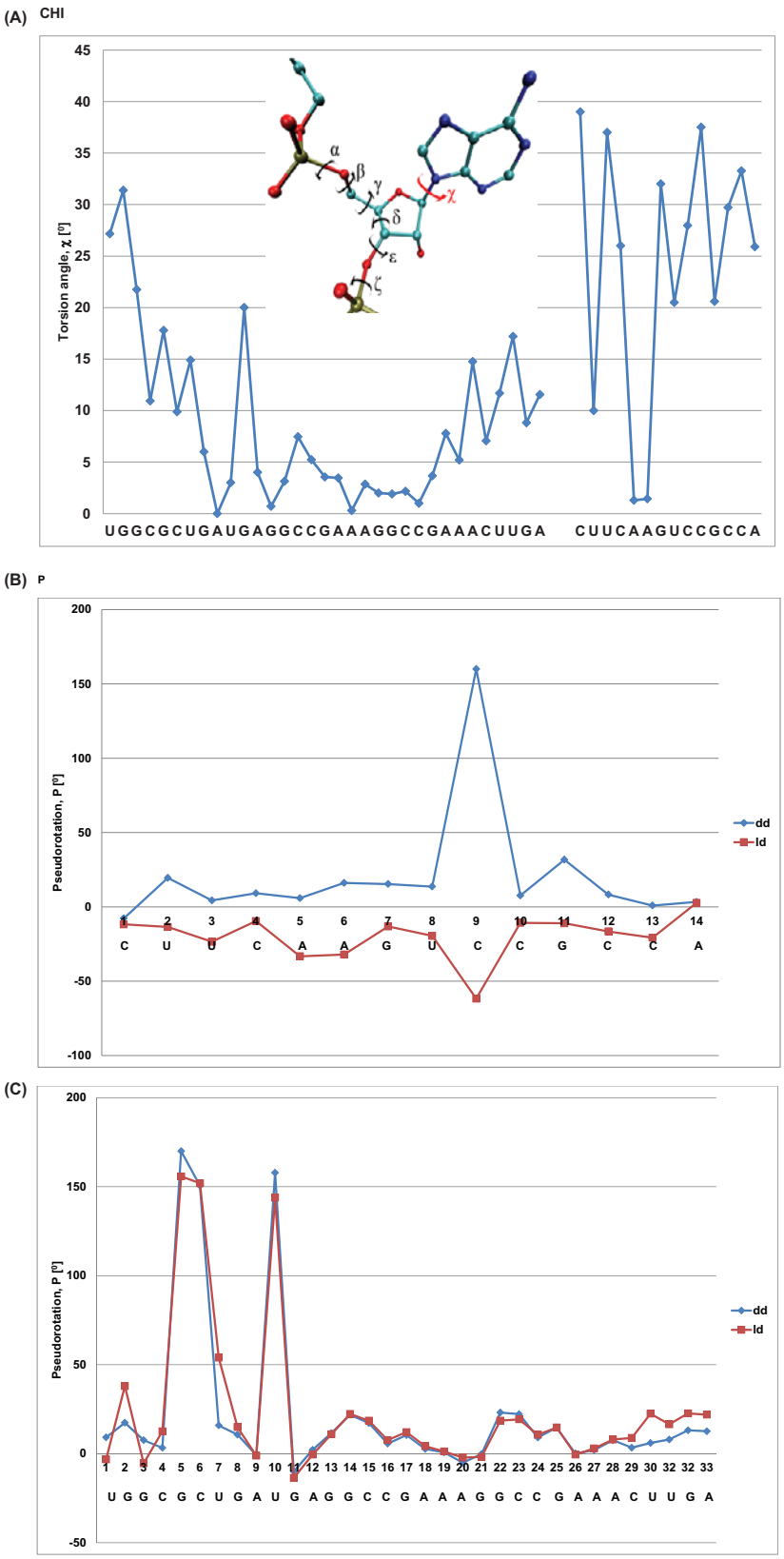

Figure 8. Differences of values of (Chi) torsion angle (A) and pseudorotation (P) angle (B and C) for homo- and heterochiral complexes; (B) RNA substrate, (C) - L-ribozyme dd – homochiral complex; ld – heterochiral complex

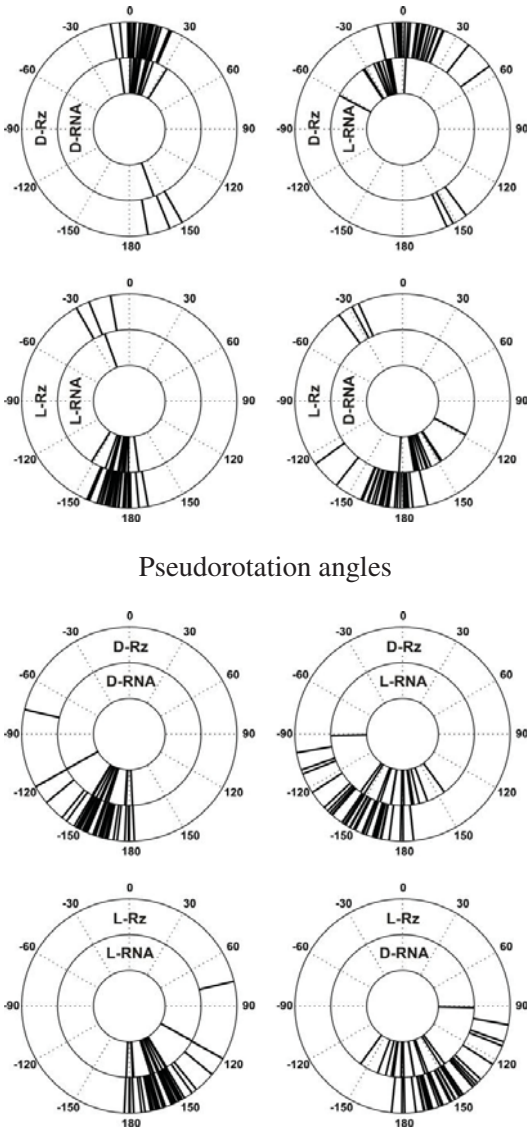

Figure 9. Circular diagram of pseudo rotation torsion and chi angle values for the target and hammerhead ribozyme molecules, in all homo- and heterochiral duplexes

are correlated with the structure of the ribozyme and show small conformational changes within the helixes 1 and 3 as well as in the active site. One should keep in mind that stem 2 (helix 2), due to its homochirality contains 4 G-C base pairs and is very stable. It is responsible for the active site formation. It seems that pairing of the substrate with flanking parts of the ribozyme is required for specificity of ribozyme cleavage and stabilization of the complex.

Next, we checked the phase pseudorotation (P) and the chi angle values of the calculated heterochiral complex. The violin plot analysis of the molecular dynamics simulation of the D-RNA/L-Rz complex with positional restraints shows that all nucleotides of the L-Rz adopt C2′-endo sugar pucker (S-type) with pseudororation phase values (P) of approximately 180^0 (Figure 10). This supports the stable conformation of left-handed ribozyme. The conformation of nucleotides of D-RNA substrate show different, mixed P values. These changes occur regularly. At the 3′-end of D-RNA nucleotides U8, C10, C12 and U14 show 2′ endo (S-type) sugar puckers, but C4, C9, C11 and C13 show 3′-endo (N-type). All the bases of the L-ribozyme are in the anti-conformation with chi angle values of approximately 160^0. Each of the second nucleotide of D-RNA substrate occurs in anti- and syn-conformation (Figure 10). These

Bioscience Reports (2021) **41** BSR20203424
https://doi.org/10.1042/BSR20203424

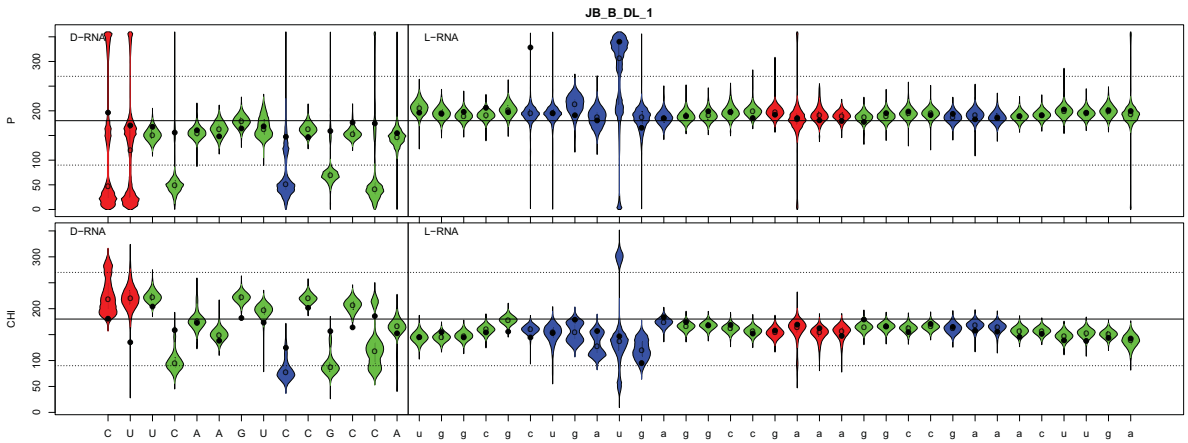

Figure 10. The violin plot analysis of pseudorotation phase (P) and chi angle values of D-RNA/L-RNA ribozyme complex. Red – single strand nucleosides, green – paired nucleosides, blue – single stranded catalytic centre

D-DNA - capital, L-RNA – small letters.

results suggest that the solution structure of the D-RNA/L-ribozyme heterochiral complex is similar to that of Z-RNA [33,34].

Discussion

The molecular structures can be chiral, and have mirror-image isomers of the opposite chirality. These isomers are called enantiomers or optical isomers, because they rotate plane-polarized light either to the right (D) or to the left (L). The building blocks of the life are homochiral, which means that naturally occurring amino acids, protein, sugars, and nucleic acids exist as only one chiral form. If these building blocks had mixed chirality, molecular chaos would ensue, and life would not be possible.

In principle, mirror-image or looking-glass versions of chiral molecules should work in the same way as original ones, but they are resistant to attack by viruses or enzymes that have not evolved in a glass-looking world. That suggestion opens the door to a new dimension of mirror-image molecular biology with broad applications in diagnostics and therapeutics. During last 40 years there have been many studies showing the formation of complexes of two strands of opposite chriality; however, the conclusions drawn from their structure are not clear [13].

In this work, we were interested in the structure of mirror image catalytic RNAs (L-RNA) and its interaction with RNA of reciprocal chirality (D-RNA). We concentrated on chemistry of the ribozyme because a specific RNA (heterochiral or homochiral) hydrolysis is based on two important premises: (i) the tertiary structure of the active center should allow the substrate to adopt a precise conformation and formation of a transient active structure, and (ii) the active site of both the homochiral and heterochiral complexes should be very similar to perform the same specific catalysis.

The D-hammerhead ribozyme activity against various D-RNAs (D-targets) has been studied recently [14,15,30–32]. The crystal structure of the D-hammerhead ribozyme (3ZP8) shows that the catalytic core adopts a well-defined structure that places the nucleophile 2′-oxygen of the target nucleotide in position for an in-line attack [28,29]. Recently, we have shown that the ribozyme specificity in the homochiral complexes (D/D and L/L) as well heterochiral (L/D and D/L) where the substrate and ribozyme have different structure (length size) is totally preserved and occurs at the predetermined GUC↓N cleavage site of the substrate [14,15]. Therefore, it is obvious that the catalytic site of the homochiral and heterochiral complexes should follow similar folding patterns. Similarly to homochiral complex, formation of the avctive heterochiral counterpart can take place only in the presence of magnesium ions (Figures 2 and 3).

Binding of D-RNA to L-Rz was observed on the gel (Figure 3 lane 2), but only after addition of Mg^{+2} ions, specific hydrolysis takes place. One can also see that L-HHRz binds to D-anti-HHRz (Figure 3, lane 4) by Mg^{+2} was not enough for hydrolysis. It seems that very stable structure of both molecules did not allow them to aquire of the active conformation.

In the CD spectra recorded for the annealed ribozyme-substrate complexes, the change in amplitude at 265 nm relative to the mathematical sum of both strands reflects conformational variation resulting from the formation of antiparallel heterochiral complexes (Figure 4A,B).

Additionally, we performed a control experiment in which we have used D-RNA substrate strand with the sequence 5′GGCGACCGACUGU3′ not fully complementary to L-Rz (ribozyme). After binding to the substrate to L-Rz, no change of the intensity of the CD signals was detected indicating that in this case the heterochiral complex did not form (Figure 4C).

Analysis of NMR spectra fully confirmed the formation of heterochiral L-Rz/D-RNA complex. New imino signals in the range of 13.5–14.5 ppm were observed in NMR spectrum when L-Rz and L-RNA/D-RNA was annealed (Figure 5).

We have also consider parallel complex formation of D-RNA target with L-HH ribozyme. However NMR spectra of such complex (Supplementary Figure S1) did not show down-field imine protons (Supplementary Figure S2), and therefore did not support a parallel helices 1 and 3.

Our 3D structure of the heterochiral models evidently shows that Watson-Crick base pairs between the ribozyme and substrate can be form although their geometry are slightly different (Figure 6C,D).

It is interesting that using standard, well-known modeling tools and simple mathematical operation one can get antiparallel heterochiral Watson–Crick base pairs, that have geometry that is very similar with the canonical Watson–Crick base pairs (Figure 6C,D). As one can see within the complex of L-hammerhead ribozyme with D-RNA, the most important helices are H1 and H3 as well as the catalytic center (Figure 1). Helix 2 (stem 2) of the D- or L-hammerhead ribozymes are always homochiral and very stable due to 4 consecutive G-C pairs [31]. Helix H2 in L-RNA is also left handed (homochiral), when in the complex with the D-RNA target. It is known that almost all nucleotides of the L-ribozyme show S configuration of ribose and anti-conformation of glycosidic bond (chi angle). Only 3 nucleotides have the N conformation in the single-stranded region, which is typical for D-RNA. Formation of Watson-Crick base pairs within the helices 1 and 3 show S configuration for L-nucleotides of ribozyme and also for D-nucleotides of RNA-target [32]. That changes of N to S of nucleotide conformation in the RNA target was induced by the stable structure of L-ribozyme (helix 2). Such a conformation is not surprising; an one can observe that for example in Z-RNA [12,17,34]. Cytidines in Z-RNA shows S configuration of sugar in nucleotides and anti conformation of nucleotides. On the other hand guanine shows N configuration of sugar and syn conformation of nucleotides [28]. One should mention here that in the heteroduplex of DNA–RNA, there are also different sugar puckers. The sugar puckers were predominantly either 3′ endo (A-RNA or DNA) or 2′ endo (B-DNA). In the heteroduplex DNA–RNA the distance between the neighboring phosphorus (P) atoms and orientation of the P relative to the sugar are different. They are 5.9 Å for C3′ exo (N) and 7.0 Å for C2′ endo (S) conformations, respectively.

To obtain deeper structural insight into the heterochiral complexes, we studied the molecular dynamics simulations of the complexes. These results suggest that the Watson-Crick like type pairing formed by strands of reversed chirality in helixes 1 and 3, are induced and stabilized by the homochiral helix 2 of the ribozyme. Such interactions maintain the active center of the catalytic RNA. Pairing between flanking L-nucleosides of ribozyme and D-RNA substrate is possible due to changes within sugar puckers and syn-anti conformation changes, which occur regularly every second nucleoside (Figure 10). Our results on heterochiral complex formation between oligo RNA of reversed chirality with different lengths confirm earlier observations on the formation heterochiral complexes [10]. In our case L-ribozyme (33 nt) binds and cleaves D-RNA of 14 nt, but previous work showed heterochiral complex of L-(dA_5)A with D-poly (U), [10]. That observation provides arguments the against current understanding that heterochiral specific Watson–Crick base pairs are not possible [8].

Competing Interests

The authors declare that there are no competing interests associated with the manuscript.

Funding

The study were supported by [grant numbers NCN OPUS 2015/17/B/ST5/01467 and SONATINA 2 2018/28/C/NZ1/00497].

Author Contribution

E.W., M.P. and J.B. designed the study and analysed data. E.W. performed the wet experiments and CD study. M.P and J.S. performed the *in silico* study. D.G. carried out and the NMR investigation. A.B and K.R. performed experiments. P.S. carried out the CD spectra measurements. E.W., D.G., J.S., A.B., P.P. and K.R. contributed to write manuscript. J.B., M.P. and E.W. wrote the manuscript.

Acknowledgements

The authors thank very much Professor Zofia Gdaniec for critical comments.

Abbreviations

CD, circular dichroism; L-Rz, L-HH, left-handed hammerhead ribozyme; NMR, nuclear magnetic resonance; siRNA, short interference RNA.

References

1 Damha, M.J., Giannaris, P.A. and Marfey, P. (1994) Antisense L/D-oligodeoxynucleotide chimeras: nuclease stability, base-pairing properties, and activity at directing ribonuclease H. *Biochemistry* **33**, 7877–7885, https://doi.org/10.1021/bi00191a015
2 Garbesi, A., Capobianco, M.L., Colonna, F.P., Tondelli, L., Arcamone, F., Manzini, G. et al. (1993) L-DNAs as potential antimessenger oligonucleotides: a reassessment. *Nucleic Acids Res.* **21**, 4159–4165, https://doi.org/10.1093/nar/21.18.4159
3 Gaglione, M. and Messere, A. (2010) Recent progress in chemically modified siRNAs. *Mini Rev. Med. Chem.* **10**, 578–595, https://doi.org/10.2174/138955710791384036
4 Vater, A. and Klussmann, S. (2015) Turning mirror-image oligonucleotides into drugs: the evolution of Spiegelmer(®) therapeutics. *Drug Discov. Today* **20**, 147–155
5 Blommers, M.J.J., Tondelli, L. and Garbesi, A. (1994) Effects of the introduction of L-nucleotides into DNA. Solution structure of the heterochiral duplex d(G-C-G-(L)T-G-C-G).d(C-G-C-A-C-G-C) studied by NMR spectroscopy. *Biochemistry* **33**, 7886–7896, https://doi.org/10.1021/bi00191a016
6 Urata, H., Ueda, Y., Suhara, H., Nishioka, E. and Akagi, M. (1993) NMR study of a heterochiral DNA: stable Watson-Crick-type base-pairing between the enantiomeric residues. *J. Am. Chem. Soc.* **115**, 9852–9853, https://doi.org/10.1021/ja00074a083
7 Szabat, M., Gudanis, D., Kotkowiak, W., Gdaniec, Z., Kierzek, R. and Pasternak, A. (2016) Thermodynamic Features of Structural Motifs Formed by β-L-RNA. *PLoS ONE* **11**, 1–11
8 Hoehlig, K., Bethge, L. and Klussmann, S. (2015) Stereospecificity of oligonucleotide interactions revisited: no evidence for heterochiral hybridization and ribozyme/DNAzyme activity. *PLoS ONE* **10**, e0115328, https://doi.org/10.1371/journal.pone.0115328
9 Fujimori, S., Shudo, K. and Hashimoto, Y. (1990) Enantio-DNA recognizes complementary RNA but not complementary DNA. *J. Am. Chem. Soc.* **112**, 7436–7438, https://doi.org/10.1021/ja00176a077
10 Ashley, G.W. (1992) Modeling, synthesis, and hybridization properties of (L)-ribonucleic acid. *J. Amer. Chem. Soc.* **114**, 9721–9736, https://doi.org/10.1021/ja00051a001
11 Sczepanski, J.T. and Joyce, G.F. (2013) Binding of a structured D-RNA molecule by an L-RNA aptamer. *J. Am. Chem. Soc.* **135**, 13290–13293, https://doi.org/10.1021/ja406634g
12 Dey, S. and Sczepanski, J.T. (2020) In vitro selection of l-DNA aptamers that bind a structured d-RNA molecule. *Nucleic Acids Res.* **48**, 1669–1680, https://doi.org/10.1093/nar/gkz1236
13 Young, B.E., Kundu, N. and Sczepanski, J.T. (2019) Mirror-Image Oligonucleotides: History and Emerging Applications. *Chemistry* **25**, 7981–7990, https://doi.org/10.1002/chem.201900149
14 Wyszko, E., Szymanski, M., Zeichhardt, H., Mueller, F., Barciszewski, J. and Erdmann, V.A. (2013) Spigelzymes: Sequence Specific Hydrolysis with Mirror Image Hammerhead Ribozymes and DNAzymes. *PLoS ONE* **8**, e54741, https://doi.org/10.1371/journal.pone.0054741
15 Wyszko, E., Mueller, F., Gabryelska, M., Bondzio, A., Popenda, M., Barciszewski, J. et al. (2014) Spiegelzymes Mirror Image Hammerhead Ribozymes and Mirror Image DNAzymes, an Alternative to siRNAs and microRNAs to Cleave mRNAs *In vivo*? *PLoS ONE* **9**, e86673, https://doi.org/10.1371/journal.pone.0086673
16 Popenda, M., Szachniuk, M., Antczak, M., Purzycka, K.J., Lukasiak, P., Bartol, N. et al. (2012) Automated 3D structure composition for large RNAs. *Nucleic Acids Res.* **40**, e112, https://doi.org/10.1093/nar/gks339
17 Gabryelska, M.M., Wyszko, E., Szymański, M., Popenda, M. and Barciszewski, J. (2013) Prediction of hammerhead ribozyme intracellular activity with the catalytic core fingerprint. *Biochem. J.* **451**, 439–451, https://doi.org/10.1042/BJ20121761
18 X-plor, Version 3. XX
19 Weiner, S.J., Kollman, P.A., Case, D.A., Singh, U.C., Ghio, C., Alagona, G. et al. (1984) A new force field for molecular mechanical simulation of nucleic acids and proteins. *J. Am. Chem. Soc.* **106**, 765–784, https://doi.org/10.1021/ja00315a051
20 Perez, A., Marchan, I., Svozil, D., Sponer, J., Cheatham, 3rd, T.E., Laughton, C.A. et al. (2007) Refinement of the AMBER force field for nucleic acids:improving the description of alpha/gamma conformers. *Biophys. J.* **92**, 3817–3829, https://doi.org/10.1529/biophysj.106.097782
21 Pettersen, E.F., Goddard, T.D., Huang, C.C., Couch, G.S., Greenblatt, D.M., Meng, E.C. et al. (2004) UCSF Chimera–a visualization system for exploratory research and analysis. *J. Comput. Chem.* **25**, 1605–1612, https://doi.org/10.1002/jcc.20084
22 Berman, H.M., Westbrook, J., Feng, Z., Gilliland, G., Bhat, T.N., Weissig, H. et al. (2000) The Protein Data Bank. *Nucleic Acids Res.* **28**, 235–242, https://doi.org/10.1093/nar/28.1.235
23 Case, D.A., Ben-Shalom, I.Y., Brozell, S.R., Cerutti, D.S., Cheatham, III, T.E. and Cruzeiro, V.W.D. (2018) *AMBER 2018*, University of California, San Francisco
24 Cornell, W.D., Cieplak, P., Bayly, Ch.I., Gould, I.R., Merz, K.M., Ferguson, D.M. et al. (1995) A second generation force field for the simulation of proteins, nucleic acids, and organic molecules. *J. Am. Chem. Soc.* **117**, 5179–5197, https://doi.org/10.1021/ja00124a002

25 Zgarbová, M., Otyepka, M., Šponer, J., Mládek, A., Banáš, P., Cheatham, III, T.E. et al. (2011) Refinement of the Cornell et al. Nucleic acids force field based on reference quantum chemical calculations of glycosidic torsion profiles. *J. Chem. Theory Comput.* **7**, 2886–2902, https://doi.org/10.1021/ct200162x
26 Jorgensen, W.L., Chandrasekhar, J., Madura, J.D., Impey, R.W. and Klein, M.L. (1983) Comparison of simple potential functions for simulating liquid water. *J. Chem. Phys.* **79**, 926–935, https://doi.org/10.1063/1.445869
27 Joung, I.S. and Cheatham, T.E. (2008) Determination of alkali and halide monovalent ion parameters for use in explicitly solvated biomolecular simulations. *J. Phys. Chem. B* **112**, 9020–9041, https://doi.org/10.1021/jp8001614
28 Anderson, M., Schultz, E.P., Martick, M. and Scott, W.G. (2013) High-resolution full-length hammerhead ribozyme. *J. Mol. Biol.* **425**, 3790, https://doi.org/10.1016/j.jmb.2013.05.017
29 Lilley, D.M.J (2019) Classification of the nucleolytic ribozymes based upon catalytic mechanism. *F1000Res* **8**, pii: F1000 Faculty Rev–1462, https://doi.org/10.12688/f1000research.19324.1
30 Dudek, M. and Trylska, J. (2017) Molecular dynamics simulations of l-RNA involving homo and heterochiral complexes. *J. Chem. Theory Comput.* **13**, 1244–1253, https://doi.org/10.1021/acs.jctc.6b01075
31 de la Peña, M., García-Robles, I. and Cervera, A. (2017) The Hammerhead Ribozyme: A Long History for a Short RNA. *Molecules* **22**, pii: E78, https://doi.org/10.3390/molecules22010078
32 Sokoloski, J.E., Godfrey, S.A., Dombrowski, S.E. and Bevilacqua, P.C. (2011) Prevalence of syn nucleobases in the active sites of functional RNAs. *RNA* **17**, 1775–1787, https://doi.org/10.1261/rna.2759911
33 Davis, P.W., Adamiak, R.W. and Tinoco, Jr, I. (1990) Z-RNA: the solution NMR structure of r(CGCGCG). *Biopolymers* **29**, 109–122, https://doi.org/10.1002/bip.360290116
34 Popenda, M., Milecki, J. and Adamiak, R.W. (2004) High salt solution structure of a left-handed RNA double helix. *Nucleic Acids Res.* **32**, 4044–4054, https://doi.org/10.1093/nar/gkh736

D- or L-RNA

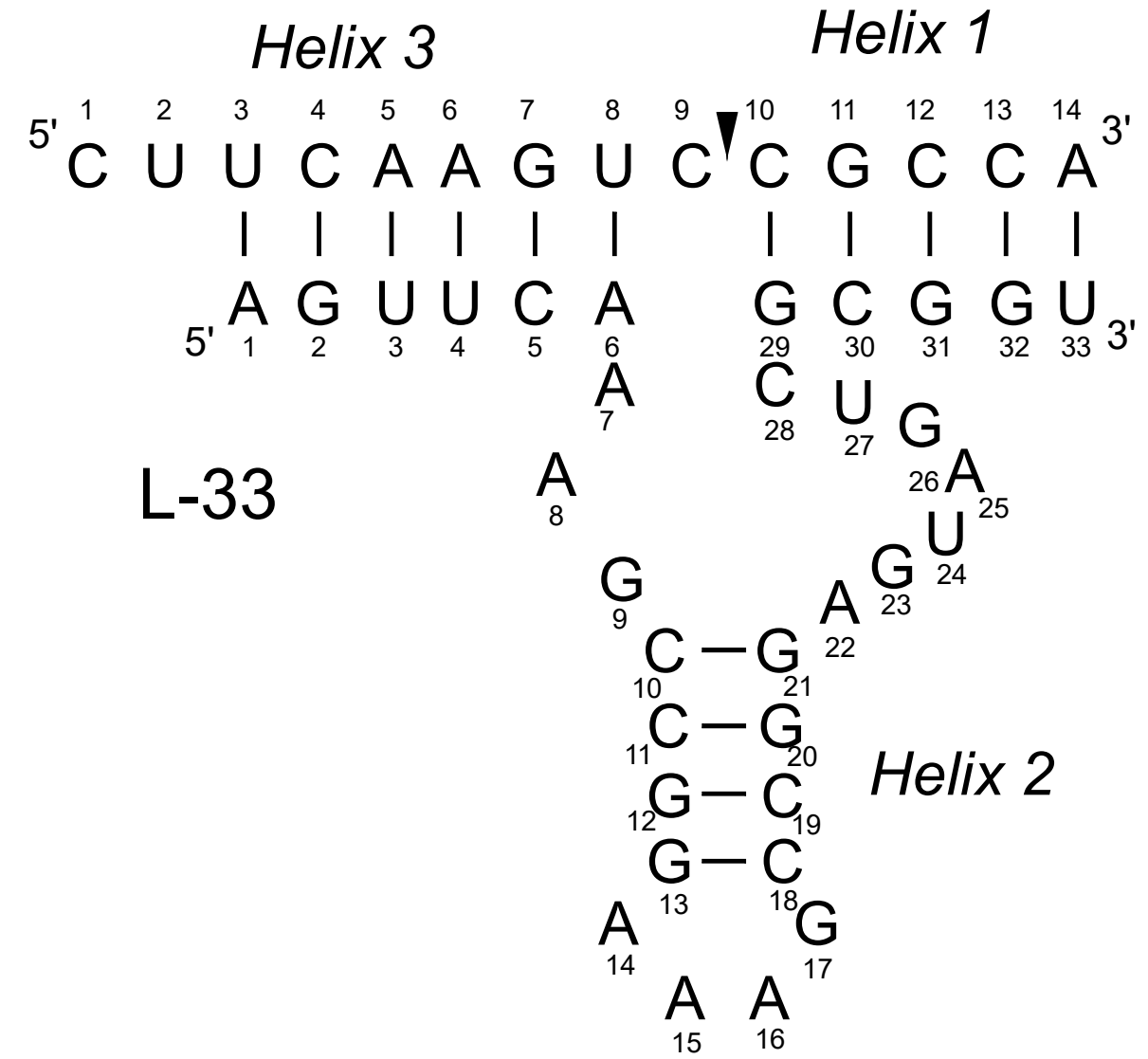
Helix 3
Helix 1
5' 1 2 3 4 5 6 7 8 9 10 11 12 13 14 3'
C U U C A A G U C C G C C A
A G U U C A G C G G U 3'
5' 1 2 3 4 5 6 29 30 31 32 33
L-33
Helix 2

Supplementary Figure 1. The secondary structure model of L-Rz/D-RNA putative parallel complex. The both nucleic acid strands run parallel from 5’ to 3’ end. Residues of 1-6 and 29-33 are 2’-O-CH_3 analogues.

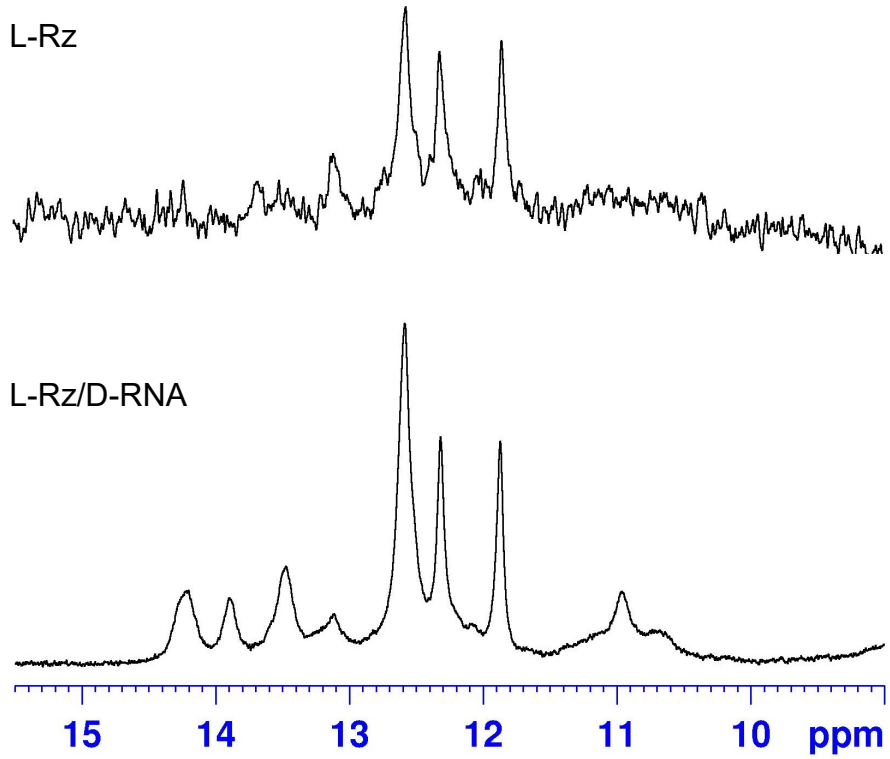
L-Rz
L-Rz/D-RNA
15
14
13
12
11
10
ppm

Supplementary Figure 2. ^{1}H NMR spectrumof the putative parallel complex of L-Rz and D-RNA.D-RNA target, L-Rz alone and L-Rz/D-RNA parallel complex with 150 mM sodium chloride, 10 mM phosphate sodium buffer pH 6.8 and 0.1 mM EDTA.

Supplementary Fig. 3.

D-target / D-ribozyme

					alpha	beta	gamma	delta	v0	v1	v2	v3	v4	P	fi	chi	epsi	zeta
1	A	1	C	c	.....	.....	21.366	90.226	17.627	-35.063	38.302	-29.235	7.446	-7.734	38.653	-176.509	-111.026	-63.033
2	A	2	U	U	-46.787	153.260	54.614	82.240	-0.583	-22.696	36.023	-37.437	23.921	19.493	38.213	-160.081	-141.569	-58.962
3	A	3	U	U	-68.174	176.487	47.443	86.061	9.744	-30.318	38.280	-33.747	15.188	4.307	38.389	-156.899	-154.743	-64.293
4	A	4	C	C	-63.419	-168.774	35.807	83.824	6.584	-28.629	38.614	-35.899	18.514	9.178	39.114	-152.727	-154.947	-77.075
5	A	5	A	A	-56.952	-179.178	39.213	85.106	8.801	-29.940	38.553	-34.581	16.317	5.850	38.755	-148.829	-154.722	-71.277
6	A	6	A	A	-64.714	169.374	58.132	82.239	1.740	-24.926	37.312	-37.383	22.470	16.120	38.839	-160.765	-155.226	-74.293
7	A	7	G	G	-69.731	179.326	54.871	83.841	2.219	-24.542	36.234	-36.022	21.332	15.341	37.573	-155.639	-156.622	-59.029
8	A	8	U	U	-72.061	-166.985	42.143	86.780	3.167	-23.695	34.008	-33.268	19.007	13.647	34.996	-149.772	-125.579	-80.833
9	A	9	C	C	-49.994	179.794	44.694	141.940	-23.128	35.618	-33.805	21.594	0.744	159.986	35.978	-119.223	-110.108	87.206
10	A	10	C	C	78.990	-141.368	-75.633	85.054	7.454	-28.578	37.724	-34.512	17.094	7.640	38.062	-162.605	-125.778	-78.259
11	A	11	G	G	-80.927	147.103	83.618	81.370	-8.832	-15.334	32.154	-38.145	29.542	31.728	37.803	177.494	-154.920	-64.279
12	A	12	C	C	-74.374	-163.385	40.445	84.984	7.077	-28.397	37.737	-34.751	17.497	8.218	38.129	-149.326	-124.839	-82.385
13	A	13	C	C	-88.733	115.061	106.604	86.786	12.038	-31.873	38.565	-32.679	13.085	0.895	38.569	-177.337		
14	A	14	A	A	-74.069	-162.507	45.198	86.712	10.270	-30.383	37.838	-33.021	14.428	3.340	37.902	-162.724	-70.740	-30.014
15	B	1	U	u	.....	.....	57.917	86.080	6.279	-27.184	36.563	-34.007	17.538	9.129	37.032	-163.467	-160.732	-57.819
16	B	2	G	G	-69.475	-162.123	37.766	81.471	0.855	-24.546	37.548	-38.127	23.452	17.384	39.345	-154.141	-133.265	-79.203
17	B	3	G	G	-92.980	121.417	111.047	86.319	7.235	-27.612	36.362	-33.277	16.470	7.584	36.683	-179.582	-145.097	-67.763
18	B	4	C	C	-68.609	-173.708	44.451	86.649	10.354	-30.554	38.064	-33.169	14.438	3.273	38.126	-156.942	-150.889	-74.422
19	B	5	G	G	-64.480	-172.070	61.889	146.574	-18.233	34.282	-36.392	26.971	-5.696	169.951	36.959	-129.649	-165.887	-108.997
20	B	6	C	C	-67.396	-175.810	43.612	138.742	-30.431	40.415	-34.669	18.156	7.501	150.572	39.805	-119.443	-88.370	154.595
21	B	7	U	U	-80.029	111.864	76.116	84.754	1.832	-23.626	35.183	-35.167	21.026	15.846	36.573	-152.242	-147.487	-47.501
22	B	8	G	G	152.385	149.229	60.567	85.197	5.263	-26.505	36.476	-34.529	18.496	10.722	37.124	179.958	-135.643	-68.930
23	B	9	A	A	-59.584	169.384	42.132	85.583	13.886	-34.393	40.748	-33.792	12.663	-0.833	40.752	-160.222	-114.470	-69.838
24	B	10	U	U	-7.844	-137.265	41.712	139.671	-24.288	36.031	-33.499	20.534	2.147	157.867	36.163	-141.336	-80.687	59.751
25	B	11	G	G	-128.453	-165.461	52.811	93.611	17.874	-33.483	35.575	-26.357	5.514	-10.091	36.134	-76.689	-155.810	99.913
26	B	12	A	A	-48.652	140.079	38.378	87.198	10.988	-30.667	37.635	-32.401	13.583	2.140	37.662	177.297	-127.770	-64.205
27	B	13	G	G	-62.861	166.158	54.154	82.511	4.992	-27.893	38.933	-37.129	20.265	11.560	39.739	-173.510	-158.088	-71.101
28	B	14	G	G	-62.527	-172.737	49.002	80.561	-2.284	-22.141	36.749	-39.107	26.046	21.826	39.587	-167.878	-149.165	-71.564
29	B	15	C	C	-83.511	170.006	71.328	81.767	0.992	-24.562	37.456	-37.915	23.253	17.168	39.202	-165.707	-158.311	-71.753
30	B	16	C	C	-66.411	-166.741	38.710	85.536	8.909	-29.894	38.384	-34.359	16.092	5.631	38.570	-151.287	-153.911	-59.607
31	B	17	G	G	-69.482	-175.912	45.580	83.599	5.690	-27.922	38.303	-36.122	19.198	10.433	38.947	-155.190	-142.321	-63.266
32	B	18	A	A	144.611	154.520	62.997	88.616	10.229	-29.227	36.033	-31.244	13.336	2.645	36.072	-171.537	-141.592	-67.299
33	B	19	A	A	-73.744	161.422	66.845	89.134	11.486	-30.159	36.325	-30.801	12.281	0.736	36.328	-164.032	-157.899	-51.759
34	B	20	A	A	-78.586	-164.728	45.923	91.301	14.997	-32.116	36.084	-28.543	8.669	-5.094	36.227	-144.394	-137.327	-80.967
35	B	21	G	G	120.757	-120.675	-160.908	88.132	12.608	-31.902	38.009	-31.870	12.251	-0.191	38.010	-177.614	-145.813	-64.435
36	B	22	G	G	-66.079	-178.400	53.428	81.092	-3.145	-20.995	35.720	-38.552	26.245	23.124	38.841	-167.010	-155.551	-61.680
37	B	23	C	C	-69.058	-175.907	48.491	82.190	-2.432	-20.969	35.001	-37.440	25.101	22.219	37.809	-152.722	-153.336	-73.972
38	B	24	C	C	101.884	-156.775	-129.683	84.721	6.539	-28.161	37.891	-35.195	18.080	9.050	38.369	-164.723	-145.073	-53.673
39	B	25	G	G	-67.769	163.185	64.541	83.999	2.636	-24.815	36.308	-35.847	20.940	14.710	37.538	-168.405	-167.313	-108.742
40	B	26	A	A	-57.211	-166.720	46.860	88.982	11.980	-30.670	36.650	-30.862	12.008	0.111	36.650	-161.581	-146.149	-59.852
41	B	27	A	A	-67.364	174.504	48.661	86.072	11.404	-31.763	38.959	-33.478	13.997	2.058	38.985	-156.068	-147.217	-75.234
42	B	28	A	A	-61.972	156.179	62.698	85.665	7.444	-28.391	37.364	-34.174	16.911	7.554	37.691	-160.529	-140.536	-76.901
43	B	29	C	C	-64.925	-179.689	40.847	85.806	10.506	-31.173	38.862	-33.903	14.850	3.385	38.930	-155.144	-157.121	-68.728
44	B	30	U	U	-63.304	-173.959	41.453	85.990	8.513	-29.272	37.742	-33.906	16.078	5.995	37.949	-149.143	-154.912	-77.649
45	B	31	U	U	-60.871	178.141	45.900	85.006	7.255	-28.461	37.695	-34.623	17.292	7.948	38.061	-150.496	-151.162	-77.442
46	B	32	G	G	-73.614	165.784	65.777	84.089	3.736	-25.845	36.853	-35.802	20.215	13.120	37.841	-161.707	-157.906	-56.055
47	B	33	A	A	-73.534	-160.870	37.994	84.918	3.987	-25.264	35.690	-34.500	19.274	12.585	36.568	-150.788	.....	.....

Supplementary Figure 3. The values of all angles characteristic for nucleotide conformation for the D-target/D-ribozyme.

Supplementary Fig. 4

D-target / L-ribozyme

					alpha	beta	gamma	delta	v0	v1	v2	v3	v4	P	fi	chi	epsi	zeta
1	A	1	C	c	.....	.....	164.222	146.659	-19.375	35.116	-36.601	26.458	-4.659	168.277	37.381	-144.241	13.607	142.497
2	A	2	U	U	-78.887	-94.873	-153.391	150.023	-23.339	40.503	-41.712	29.198	-3.783	166.483	42.900	170.421	-75.401	-172.580
3	A	3	U	U	8.817	-117.388	177.122	146.878	-31.210	45.305	-41.734	24.706	3.889	156.557	45.489	-166.375	-76.543	179.578
4	A	4	C	C	18.954	-139.762	-154.618	154.137	-21.027	40.115	-43.093	31.851	-6.946	170.437	43.701	-178.880	-27.506	-179.805
5	A	5	A	A	-35.403	-97.865	-156.265	135.915	-32.079	40.331	-33.142	15.635	10.124	146.741	39.635	147.522	-96.868	-126.533
6	A	6	A	A	32.259	-121.755	-154.915	131.336	-27.558	35.260	-29.300	14.385	8.057	147.935	34.574	159.336	52.774	86.271
7	A	7	G	G	91.145	130.433	139.122	153.472	-23.975	42.049	-43.314	30.557	-4.295	166.839	44.483	-172.704	-74.261	170.308
8	A	8	U	U	27.930	-138.622	-162.362	147.797	-27.578	42.721	-41.236	26.186	0.753	160.530	43.737	170.780	-89.103	-178.780
9	A	9	C	C	14.533	-100.460	-142.464	115.688	-38.274	34.049	-17.800	-3.419	26.059	118.287	37.562	91.266	-140.318	73.980
10	A	10	C	C	-104.942	157.105	-129.380	148.493	-19.568	36.256	-38.245	28.010	-5.501	169.266	38.927	-159.663	1.290	164.203
11	A	11	G	G	-81.544	-86.543	-149.807	147.391	-19.316	35.462	-37.311	27.280	-5.187	169.004	38.009	161.832	-148.536	-123.961
12	A	12	C	C	102.830	-169.643	-174.958	147.445	-24.472	40.063	-39.776	26.653	-1.533	163.462	41.493	179.044	-84.161	-174.064
13	A	13	C	C	20.369	-123.772	-155.549	142.191	-24.795	37.642	-35.636	22.304	1.418	159.251	38.108	144.063		
14	A	14	A	A	122.579	154.042	161.777	151.082	-10.431	29.934	-37.025	32.032	-13.727	-177.289	37.067	-171.022	-18.443	47.018
15	B	1	U	u	.....	.....	-30.150	-89.321	-14.337	32.553	-37.461	30.265	-10.157	176.789	37.520	135.856	149.632	73.630
16	B	2	G	G	49.832	-176.983	-47.430	-81.485	13.007	11.534	-30.058	38.364	-32.290	-142.057	38.114	123.003	151.421	47.830
17	B	3	G	G	127.835	-113.124	-136.068	-90.938	-15.433	32.675	-36.613	28.786	-8.553	174.541	36.780	157.840	145.918	61.988
18	B	4	C	C	62.413	178.813	-45.121	-83.364	-4.198	26.696	-37.783	36.446	-20.340	-167.447	38.708	146.012	148.632	72.414
19	B	5	G	G	54.253	-177.329	-61.192	-139.575	26.364	-37.868	34.378	-20.216	-3.652	-24.253	37.706	111.871	167.008	108.029
20	B	6	C	C	66.558	177.863	-41.409	-138.348	29.161	-39.497	34.419	-18.619	-6.415	-28.055	39.002	109.564	95.331	-156.438
21	B	7	U	U	85.743	-114.863	-73.967	-87.212	20.752	0.869	-20.469	32.904	-33.730	-126.060	34.773	166.293	141.847	54.719
22	B	8	G	G	-159.269	-149.195	-59.837	-84.186	-2.501	24.455	-35.857	35.489	-20.816	-165.106	37.103	-174.092	130.740	73.490
23	B	9	A	A	57.641	-170.436	-38.110	-87.955	-13.283	32.510	-38.309	31.737	-11.737	178.873	38.317	160.226	117.589	81.954
24	B	10	U	U	-2.720	149.771	-50.037	-131.620	30.899	-37.406	29.594	-12.757	-11.191	-36.232	36.688	138.811	81.007	-66.509
25	B	11	G	G	145.610	166.222	-57.092	-97.247	-18.159	31.452	-32.103	22.684	-3.043	166.410	33.027	100.076	141.106	-90.807
26	B	12	A	A	76.968	-161.162	-51.653	-88.391	-12.705	31.643	-37.555	31.352	-11.858	179.436	37.557	178.835	134.905	55.653
27	B	13	G	G	70.783	-173.665	-55.989	-83.013	-5.360	27.907	-38.601	36.579	-19.683	-169.046	39.317	172.823	157.768	68.932
28	B	14	G	G	60.248	170.333	-43.826	-80.264	2.680	21.905	-36.714	39.282	-26.401	-157.650	39.696	164.737	153.443	69.897
29	B	15	C	C	82.818	-170.541	-71.076	-82.501	-0.045	23.293	-36.361	37.376	-23.509	-161.453	38.353	158.252	158.969	70.718
30	B	16	C	C	70.138	166.520	-40.875	-85.044	-7.466	28.708	-37.865	34.639	-17.179	-172.354	38.205	145.770	151.035	61.549
31	B	17	G	G	67.505	178.460	-46.256	-83.646	-4.475	26.740	-37.580	36.084	-19.936	-167.896	38.435	158.754	143.235	61.884
32	B	18	A	A	-144.010	-151.773	-66.005	-88.061	-9.317	28.788	-36.221	31.961	-14.362	-175.784	36.319	168.074	142.551	62.504
33	B	19	A	A	77.095	-162.934	-67.330	-88.760	-11.212	30.081	-36.448	31.098	-12.641	-178.751	36.456	163.753	153.127	59.288
34	B	20	A	A	69.472	175.343	-46.558	-89.937	-13.350	31.391	-36.513	29.927	-10.569	177.836	36.539	147.238	126.420	86.797
35	B	21	G	G	-112.427	114.230	157.866	-89.034	-13.496	32.092	-37.479	30.803	-11.011	178.126	37.499	-179.726	145.904	63.339
36	B	22	G	G	63.018	175.722	-47.778	-82.389	-0.025	23.322	-36.405	37.435	-23.568	-161.423	38.407	168.556	154.708	64.725
37	B	23	C	C	64.855	177.572	-46.466	-82.788	0.437	22.613	-35.729	37.029	-23.579	-160.736	37.848	150.547	155.438	70.799
38	B	24	C	C	-105.567	157.954	132.617	-85.112	-5.394	26.873	-36.960	34.952	-18.654	-169.375	37.605	165.713	146.760	52.047
39	B	25	G	G	72.267	-172.202	-58.431	-84.484	-2.572	24.339	-35.582	35.144	-20.544	-165.277	36.790	164.749	177.474	102.057
40	B	26	A	A	55.182	163.830	-47.493	-89.910	-12.200	30.430	-36.082	30.141	-11.418	179.448	36.084	153.797	143.530	63.663
41	B	27	A	A	62.127	-170.488	-47.747	-87.105	-10.480	30.376	-37.633	32.691	-14.083	-177.075	37.682	150.866	147.901	71.223
42	B	28	A	A	67.271	-158.578	-70.648	-85.386	-7.201	28.307	-37.472	34.391	-17.194	-172.064	37.834	145.769	141.252	72.587
43	B	29	C	C	77.089	-173.161	-56.942	-83.761	-6.833	28.964	-38.855	36.005	-18.412	-171.150	39.323	148.089	157.835	62.014
44	B	30	U	U	68.637	170.888	-44.821	-81.557	2.658	21.213	-35.629	38.171	-25.698	-157.547	38.552	137.465	160.413	71.078
45	B	31	U	U	69.745	-178.743	-54.363	-83.666	-1.426	23.835	-35.875	36.106	-21.871	-163.495	37.417	133.287	156.296	69.316
46	B	32	G	G	79.973	-165.465	-70.702	-82.264	2.733	20.766	-34.963	37.546	-25.366	-157.360	37.882	152.883	157.461	61.872
47	B	33	A	A	64.325	175.082	-46.354	-82.663	2.157	20.800	-34.467	36.747	-24.521	-158.109	37.146	139.233	.....	.....

Supplementary Figure 4. The values of all angles characteristic for nucleotide conformation for the D-target/L-ribozyme.

Supplementary Fig. 5

L-target / L-ribozyme

					alpha	beta	gamma	delta	v0	v1	v2	v3	v4	P	fi	chi	epsi	zeta
1	A	1	C	c	.....	.....	-21.366	-90.226	-17.627	35.063	-38.302	29.235	-7.446	172.266	38.653	176.509	111.026	63.033
2	A	2	U	U	46.787	-153.260	-54.614	-82.240	0.583	22.696	-36.023	37.437	-23.921	-160.507	38.213	160.081	141.569	58.962
3	A	3	U	U	68.174	-176.487	-47.443	-86.061	-9.744	30.318	-38.280	33.747	-15.188	-175.693	38.389	156.899	154.743	64.293
4	A	4	C	C	63.419	168.774	-35.807	-83.824	-6.584	28.629	-38.614	35.899	-18.514	-170.822	39.114	152.727	154.947	77.075
5	A	5	A	A	56.952	179.178	-39.213	-85.106	-8.801	29.940	-38.553	34.581	-16.317	-174.150	38.755	148.829	154.722	71.277
6	A	6	A	A	64.714	-169.374	-58.132	-82.239	-1.740	24.926	-37.312	37.383	-22.470	-163.880	38.839	160.765	155.226	74.293
7	A	7	G	G	69.731	-179.326	-54.871	-83.841	-2.219	24.542	-36.234	36.022	-21.332	-164.659	37.573	155.639	156.622	59.029
8	A	8	U	U	72.061	166.985	-42.143	-86.780	-3.167	23.695	-34.008	33.268	-19.007	-166.353	34.996	149.772	125.579	80.833
9	A	9	C	C	49.994	-179.794	-44.694	-141.940	23.128	-35.618	33.805	-21.594	-0.744	-20.014	35.978	119.223	110.108	-87.206
10	A	10	C	C	-78.990	141.368	75.633	-85.054	-7.454	28.578	-37.724	34.512	-17.094	-172.360	38.062	162.605	125.778	78.259
11	A	11	G	G	80.927	-147.103	-83.618	-81.370	8.832	15.334	-32.154	38.145	-29.542	-148.272	37.803	-177.494	154.920	64.279
12	A	12	C	C	74.374	163.385	-40.445	-84.984	-7.077	28.397	-37.737	34.751	-17.497	-171.782	38.129	149.326	124.839	82.385
13	A	13	C	C	88.733	-115.061	-106.604	-86.786	-12.038	31.873	-38.565	32.679	-13.085	-179.105	38.569	177.337		
14	A	14	A	A	74.069	162.507	-45.198	-86.712	-10.270	30.383	-37.838	33.021	-14.428	-176.660	37.902	162.724	70.740	30.014
15	B	1	U	u	.....	.....	-57.917	-86.080	-6.279	27.184	-36.563	34.007	-17.538	-170.871	37.032	163.467	160.732	57.819
16	B	2	G	G	69.475	162.123	-37.766	-81.471	-0.855	24.546	-37.548	38.127	-23.452	-162.616	39.345	154.141	133.265	79.203
17	B	3	G	G	92.980	-121.417	-111.047	-86.319	-7.235	27.612	-36.362	33.277	-16.470	-172.416	36.683	179.582	145.097	67.763
18	B	4	C	C	68.609	173.708	-44.451	-86.649	-10.354	30.554	-38.064	33.169	-14.438	-176.727	38.126	156.942	150.889	74.422
19	B	5	G	G	64.480	172.070	-61.889	-146.574	18.233	-34.282	36.392	-26.971	5.696	-10.049	36.959	129.649	165.887	108.997
20	B	6	C	C	67.396	175.810	-43.612	-138.742	30.431	-40.415	34.669	-18.156	-7.501	-29.428	39.805	119.443	88.370	-154.595
21	B	7	U	U	80.029	-111.864	-76.116	-84.754	-1.832	23.626	-35.183	35.167	-21.026	-164.154	36.573	152.242	147.487	47.501
22	B	8	G	G	-152.385	-149.229	-60.567	-85.197	-5.263	26.505	-36.476	34.529	-18.496	-169.278	37.124	-179.958	135.643	68.930
23	B	9	A	A	59.584	-169.384	-42.132	-85.583	-13.886	34.393	-40.748	33.792	-12.663	179.167	40.752	160.222	114.470	69.838
24	B	10	U	U	7.844	137.265	-41.712	-139.671	24.288	-36.031	33.499	-20.534	-2.147	-22.133	36.163	141.336	80.687	-59.751
25	B	11	G	G	128.453	165.461	-52.811	-93.611	-17.874	33.483	-35.575	26.357	-5.514	169.909	36.134	76.689	155.810	-99.913
26	B	12	A	A	48.652	-140.079	-38.378	-87.198	-10.988	30.667	-37.635	32.401	-13.583	-177.860	37.662	-177.297	127.770	64.205
27	B	13	G	G	62.861	-166.158	-54.154	-82.511	-4.992	27.893	-38.933	37.129	-20.265	-168.440	39.739	173.510	158.088	71.101
28	B	14	G	G	62.527	172.737	-49.002	-80.561	2.284	22.141	-36.749	39.107	-26.046	-158.174	39.587	167.878	149.165	71.564
29	B	15	C	C	83.511	-170.006	-71.328	-81.767	-0.992	24.562	-37.456	37.915	-23.253	-162.832	39.202	165.707	158.311	71.753
30	B	16	C	C	66.411	166.741	-38.710	-85.536	-8.909	29.894	-38.384	34.359	-16.092	-174.369	38.570	151.287	153.911	59.607
31	B	17	G	G	69.482	175.912	-45.580	-83.599	-5.690	27.922	-38.303	36.122	-19.198	-169.567	38.947	155.190	142.321	63.266
32	B	18	A	A	-144.611	-154.520	-62.997	-88.616	-10.229	29.227	-36.033	31.244	-13.336	-177.355	36.072	171.537	141.592	67.299
33	B	19	A	A	73.744	-161.422	-66.845	-89.134	-11.486	30.159	-36.325	30.801	-12.281	-179.264	36.328	164.032	157.899	51.759
34	B	20	A	A	78.586	164.728	-45.923	-91.301	-14.997	32.116	-36.084	28.543	-8.669	174.906	36.227	144.394	137.327	80.967
35	B	21	G	G	-120.757	120.675	160.908	-88.132	-12.608	31.902	-38.009	31.870	-12.251	179.809	38.010	177.614	145.813	64.435
36	B	22	G	G	66.079	178.400	-53.428	-81.092	3.145	20.995	-35.720	38.552	-26.245	-156.876	38.841	167.010	155.551	61.680
37	B	23	C	C	69.058	175.907	-48.491	-82.190	2.432	20.969	-35.001	37.440	-25.101	-157.781	37.809	152.722	153.336	73.972
38	B	24	C	C	-101.884	156.775	129.683	-84.721	-6.539	28.161	-37.891	35.195	-18.080	-170.950	38.369	164.723	145.073	53.673
39	B	25	G	G	67.769	-163.185	-64.541	-83.999	-2.636	24.815	-36.308	35.847	-20.940	-165.290	37.538	168.405	167.313	108.742
40	B	26	A	A	57.211	166.720	-46.860	-88.982	-11.980	30.670	-36.650	30.862	-12.008	-179.889	36.650	161.581	146.149	59.852
41	B	27	A	A	67.364	-174.504	-48.661	-86.072	-11.404	31.763	-38.959	33.478	-13.997	-177.942	38.985	156.068	147.217	75.234
42	B	28	A	A	61.972	-156.179	-62.698	-85.665	-7.444	28.391	-37.364	34.174	-16.911	-172.446	37.691	160.529	140.536	76.901
43	B	29	C	C	64.925	179.689	-40.847	-85.806	-10.506	31.173	-38.862	33.903	-14.850	-176.615	38.930	155.144	157.121	68.728
44	B	30	U	U	63.304	173.959	-41.453	-85.990	-8.513	29.272	-37.742	33.906	-16.078	-174.005	37.949	149.143	154.912	77.649
45	B	31	U	U	60.871	-178.141	-45.900	-85.006	-7.255	28.461	-37.695	34.623	-17.292	-172.052	38.061	150.496	151.162	77.442
46	B	32	G	G	73.614	-165.784	-65.777	-84.089	-3.736	25.845	-36.853	35.802	-20.215	-166.880	37.841	161.707	157.906	56.055
47	B	33	A	A	73.534	160.870	-37.994	-84.918	-3.987	25.264	-35.690	34.500	-19.274	-167.415	36.568	150.788	.....	.....

Supplementary Figure 5. The values of all angles characteristic for nucleotide conformation for the L-target/L-ribozyme.

Supplementary Fig. 6

L-target / D-ribozyme

					alpha	beta	gamma	delta	v0	v1	v2	v3	v4	P	fi	chi	epsi	zeta
1	A	1	C	c	.....	.....	-164.222	-146.659	19.375	-35.116	36.601	-26.458	4.659	-11.723	37.381	144.241	-13.607	-142.497
2	A	2	U	U	78.887	94.873	153.391	-150.023	23.339	-40.503	41.712	-29.198	3.783	-13.517	42.900	-170.421	75.401	172.580
3	A	3	U	U	-8.817	117.388	-177.122	-146.878	31.210	-45.305	41.734	-24.706	-3.889	-23.443	45.489	166.375	76.543	-179.578
4	A	4	C	C	-18.954	139.762	154.618	-154.137	21.027	-40.115	43.093	-31.851	6.946	-9.563	43.701	178.880	27.506	179.805
5	A	5	A	A	35.403	97.865	156.265	-135.915	32.079	-40.331	33.142	-15.635	-10.124	-33.259	39.635	-147.522	96.868	126.533
6	A	6	A	A	-32.259	121.755	154.915	-131.336	27.558	-35.260	29.300	-14.385	-8.057	-32.065	34.574	-159.336	-52.774	-86.271
7	A	7	G	G	-91.145	-130.433	-139.122	-153.472	23.975	-42.049	43.314	-30.557	4.295	-13.161	44.483	172.704	74.261	-170.308
8	A	8	U	U	-27.930	138.622	162.362	-147.797	27.578	-42.721	41.236	-26.186	-0.753	-19.470	43.737	-170.780	89.103	178.780
9	A	9	C	C	-14.533	100.460	142.464	-115.688	38.274	-34.049	17.800	3.419	-26.059	-61.713	37.562	-91.266	140.318	-73.980
10	A	10	C	C	104.942	-157.105	129.380	-148.493	19.568	-36.256	38.245	-28.010	5.501	-10.734	38.927	159.663	-1.290	-164.203
11	A	11	G	G	81.544	86.543	149.807	-147.391	19.316	-35.462	37.311	-27.280	5.187	-10.996	38.009	-161.832	148.536	123.961
12	A	12	C	C	-102.830	169.643	174.958	-147.445	24.472	-40.063	39.776	-26.653	1.533	-16.538	41.493	-179.044	84.161	174.064
13	A	13	C	C	-20.369	123.772	155.549	-142.191	24.795	-37.642	35.636	-22.304	-1.418	-20.749	38.108	-144.063		
14	A	14	A	A	-122.579	-154.042	-161.777	-151.082	10.431	-29.934	37.025	-32.032	13.727	2.711	37.067	171.022	18.443	-47.018
15	B	1	U	u	.....	.....	30.150	89.321	14.337	-32.553	37.461	-30.265	10.157	-3.211	37.520	-135.856	-149.632	-73.630
16	B	2	G	G	-49.832	176.983	47.430	81.485	-13.007	-11.534	30.058	-38.364	32.290	37.943	38.114	-123.003	-151.421	-47.830
17	B	3	G	G	-127.835	113.124	136.068	90.938	15.433	-32.675	36.613	-28.786	8.553	-5.459	36.780	-157.840	-145.918	-61.988
18	B	4	C	C	-62.413	-178.813	45.121	83.364	4.198	-26.696	37.783	-36.446	20.340	12.553	38.708	-146.012	-148.632	-72.414
19	B	5	G	G	-54.253	177.329	61.192	139.575	-26.364	37.868	-34.378	20.216	3.652	155.747	37.706	-111.871	-167.008	-108.029
20	B	6	C	C	-66.558	-177.863	41.409	138.348	-29.161	39.497	-34.419	18.619	6.415	151.945	39.002	-109.564	-95.331	156.438
21	B	7	U	U	-85.743	114.863	73.967	87.212	-20.752	-0.869	20.469	-32.904	33.730	53.940	34.773	-166.293	-141.847	-54.719
22	B	8	G	G	159.269	149.195	59.837	84.186	2.501	-24.455	35.857	-35.489	20.816	14.894	37.103	174.092	-130.740	-73.490
23	B	9	A	A	-57.641	170.436	38.110	87.955	13.283	-32.510	38.309	-31.737	11.737	-1.127	38.317	-160.226	-117.589	-81.954
24	B	10	U	U	2.720	-149.771	50.037	131.620	-30.899	37.406	-29.594	12.757	11.191	143.768	36.688	-138.811	-81.007	66.509
25	B	11	G	G	-145.610	-166.222	57.092	97.247	18.159	-31.452	32.103	-22.684	3.043	-13.590	33.027	-100.076	-141.106	90.807
26	B	12	A	A	-76.968	161.162	51.653	88.391	12.705	-31.643	37.555	-31.352	11.858	-0.564	37.557	-178.835	-134.905	-55.653
27	B	13	G	G	-70.783	173.665	55.989	83.013	5.360	-27.907	38.601	-36.579	19.683	10.954	39.317	-172.823	-157.768	-68.932
28	B	14	G	G	-60.248	-170.333	43.826	80.264	-2.680	-21.905	36.714	-39.282	26.401	22.350	39.696	-164.737	-153.443	-69.897
29	B	15	C	C	-82.818	170.541	71.076	82.501	0.045	-23.293	36.361	-37.376	23.509	18.547	38.353	-158.252	-158.969	-70.718
30	B	16	C	C	-70.138	-166.520	40.875	85.044	7.466	-28.708	37.865	-34.639	17.179	7.646	38.205	-145.770	-151.035	-61.549
31	B	17	G	G	-67.505	-178.460	46.256	83.646	4.475	-26.740	37.580	-36.084	19.936	12.104	38.435	-158.754	-143.235	-61.884
32	B	18	A	A	144.010	151.773	66.005	88.061	9.317	-28.788	36.221	-31.961	14.362	4.216	36.319	-168.074	-142.551	-62.504
33	B	19	A	A	-77.095	162.934	67.330	88.760	11.212	-30.081	36.448	-31.098	12.641	1.249	36.456	-163.753	-153.127	-59.288
34	B	20	A	A	-69.472	-175.343	46.558	89.937	13.350	-31.391	36.513	-29.927	10.569	-2.164	36.539	-147.238	-126.420	-86.797
35	B	21	G	G	112.427	-114.230	-157.866	89.034	13.496	-32.092	37.479	-30.803	11.011	-1.874	37.499	179.726	-145.904	-63.339
36	B	22	G	G	-63.018	-175.722	47.778	82.389	0.025	-23.322	36.405	-37.435	23.568	18.577	38.407	-168.556	-154.708	-64.725
37	B	23	C	C	-64.855	-177.572	46.466	82.788	-0.437	-22.613	35.729	-37.029	23.579	19.264	37.848	-150.547	-155.438	-70.799
38	B	24	C	C	105.567	-157.954	-132.617	85.112	5.394	-26.873	36.960	-34.952	18.654	10.625	37.605	-165.713	-146.760	-52.047
39	B	25	G	G	-72.267	172.202	58.431	84.484	2.572	-24.339	35.582	-35.144	20.544	14.723	36.790	-164.749	-177.474	-102.057
40	B	26	A	A	-55.182	-163.830	47.493	89.910	12.200	-30.430	36.082	-30.141	11.418	-0.552	36.084	-153.797	-143.530	-63.663
41	B	27	A	A	-62.127	170.488	47.747	87.105	10.480	-30.376	37.633	-32.691	14.083	2.925	37.682	-150.866	-147.901	-71.223
42	B	28	A	A	-67.271	158.578	70.648	85.386	7.201	-28.307	37.472	-34.391	17.194	7.936	37.834	-145.769	-141.252	-72.587
43	B	29	C	C	-77.089	173.161	56.942	83.761	6.833	-28.964	38.855	-36.005	18.412	8.850	39.323	-148.089	-157.835	-62.014
44	B	30	U	U	-68.637	-170.888	44.821	81.557	-2.658	-21.213	35.629	-38.171	25.698	22.453	38.552	-137.465	-160.413	-71.078
45	B	31	U	U	-69.745	178.743	54.363	83.666	1.426	-23.835	35.875	-36.106	21.871	16.505	37.417	-133.287	-156.296	-69.316
46	B	32	G	G	-79.973	165.465	70.702	82.264	-2.733	-20.766	34.963	-37.546	25.366	22.640	37.882	-152.883	-157.461	-61.872
47	B	33	A	A	-64.325	-175.082	46.354	82.663	-2.157	-20.800	34.467	-36.747	24.521	21.891	37.146	-139.233	.....	.....

Supplementary Figure 6. The values of all angles characteristic for nucleotide conformation for the L-target/D-ribozyme.

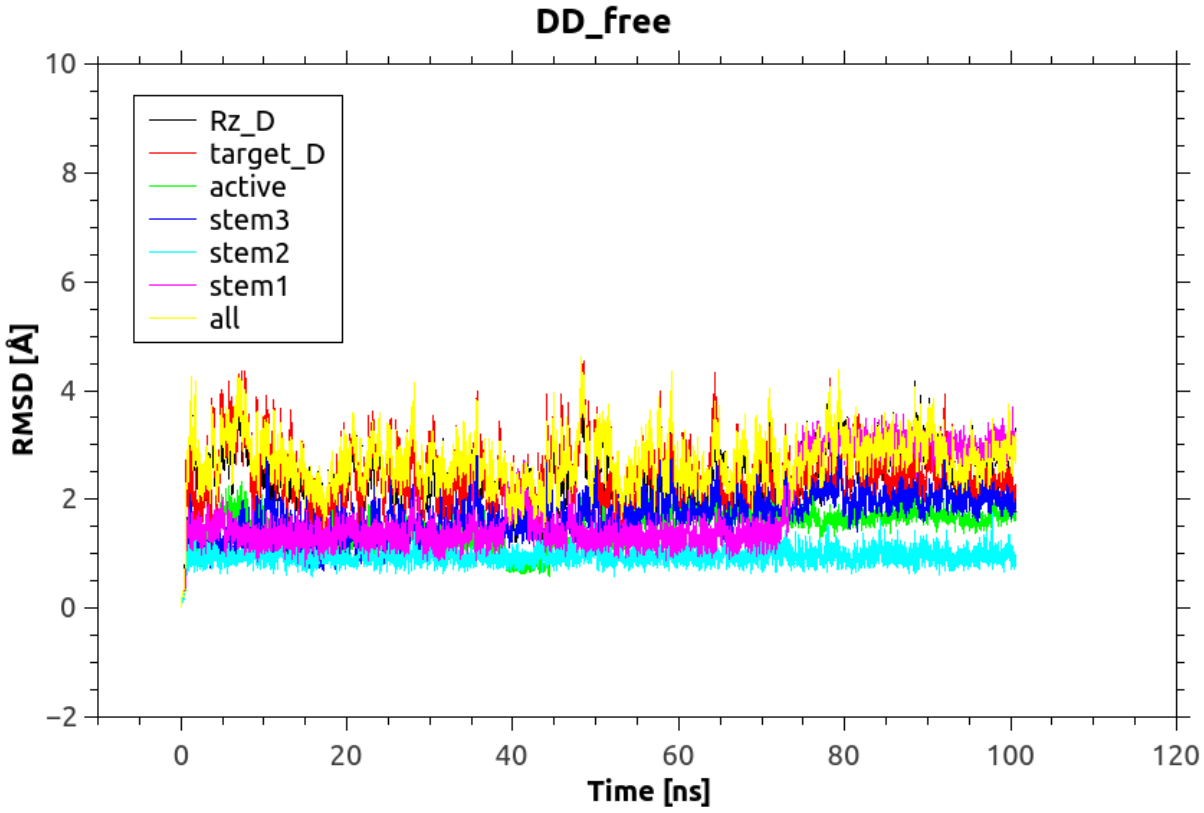
DD_free
Rz_D
target_D
active
stem3
stem2
stem1
all
RMSD [Å]
Time [ns]
10
8
6
4
2
0
−2
0
20
40
60
80
100
120

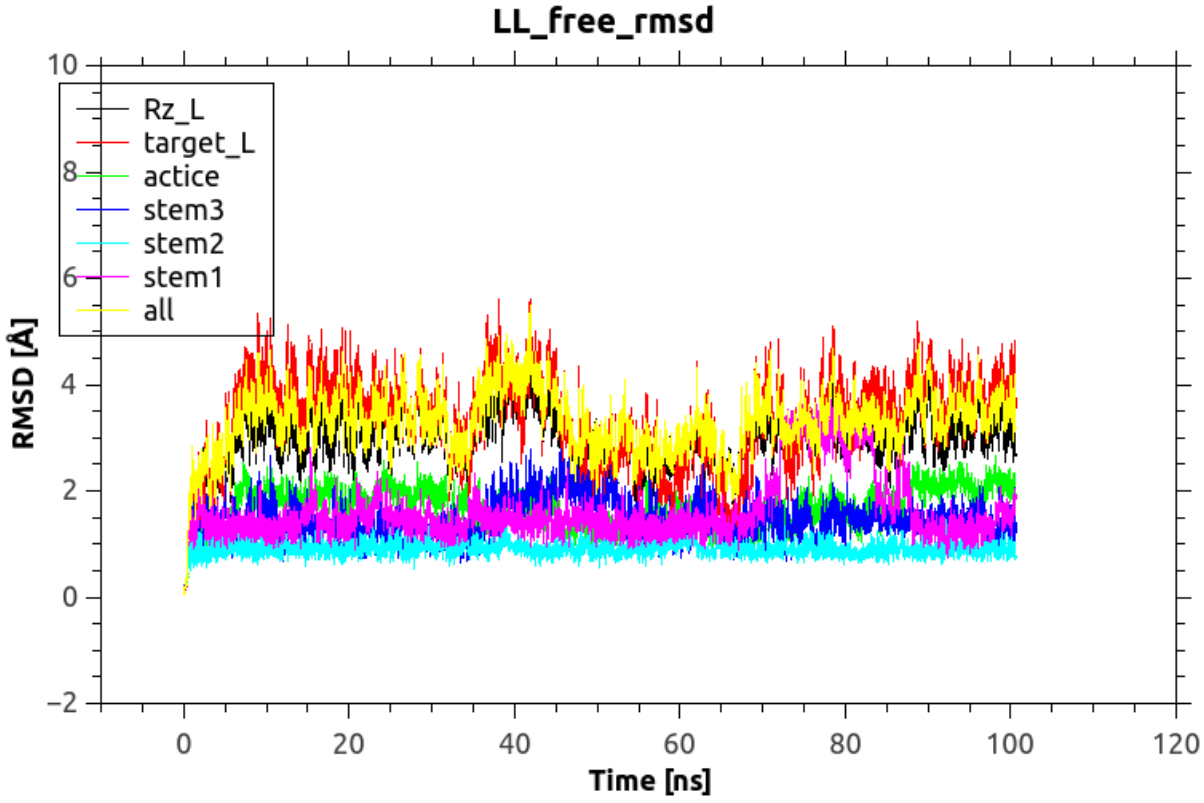
LL_free_rmsd
Rz_L
target_L
actice
stem3
stem2
stem1
all
RMSD [Å]
Time [ns]
10
8
6
4
2
0
−2
0
20
40
60
80
100
120

Supplementary Figure 7. RMSD for the whole homochiral ribozyme complexes with RNA (D/D or L/L) and their structural domains calculated without any restrains (free).

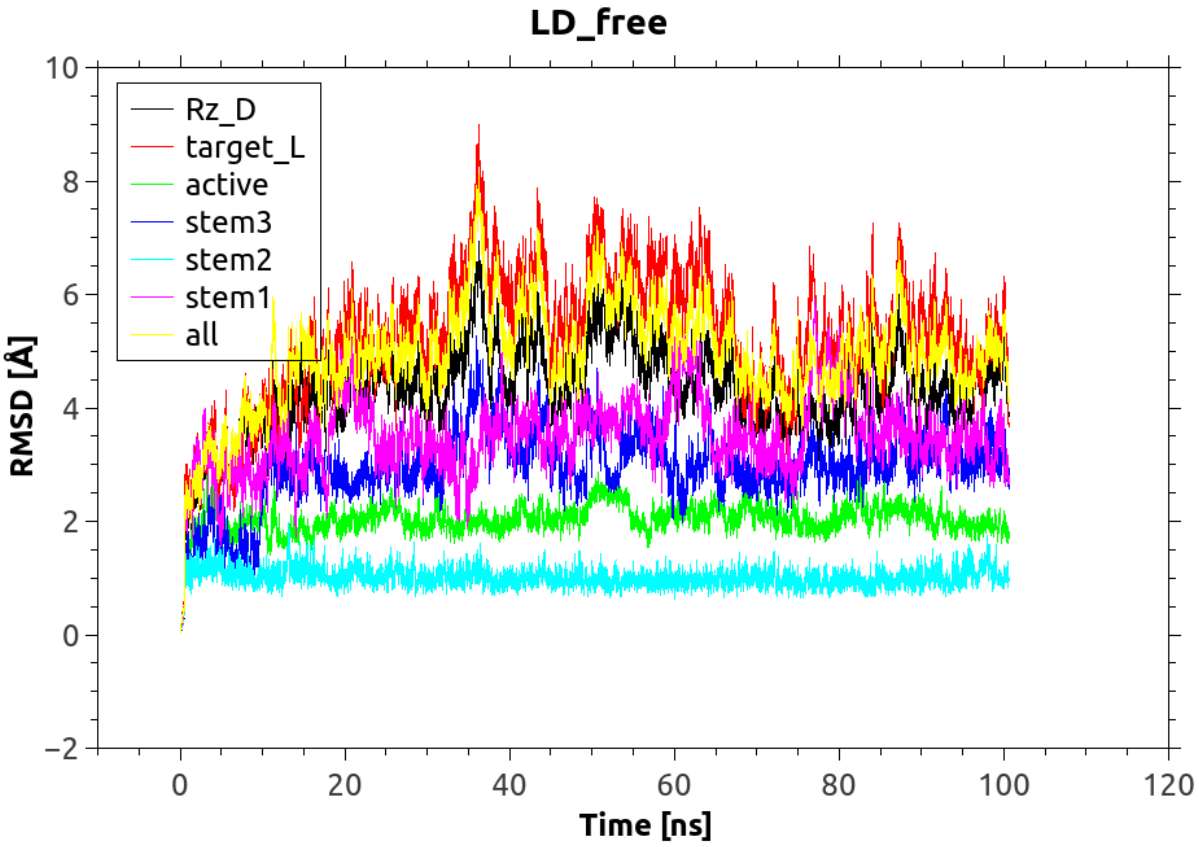
LD_free
Rz_D
target_L
active
stem3
stem2
stem1
all
RMSD [Å]
Time [ns]
10
8
6
4
2
0
−2
0
20
40
60
80
100
120

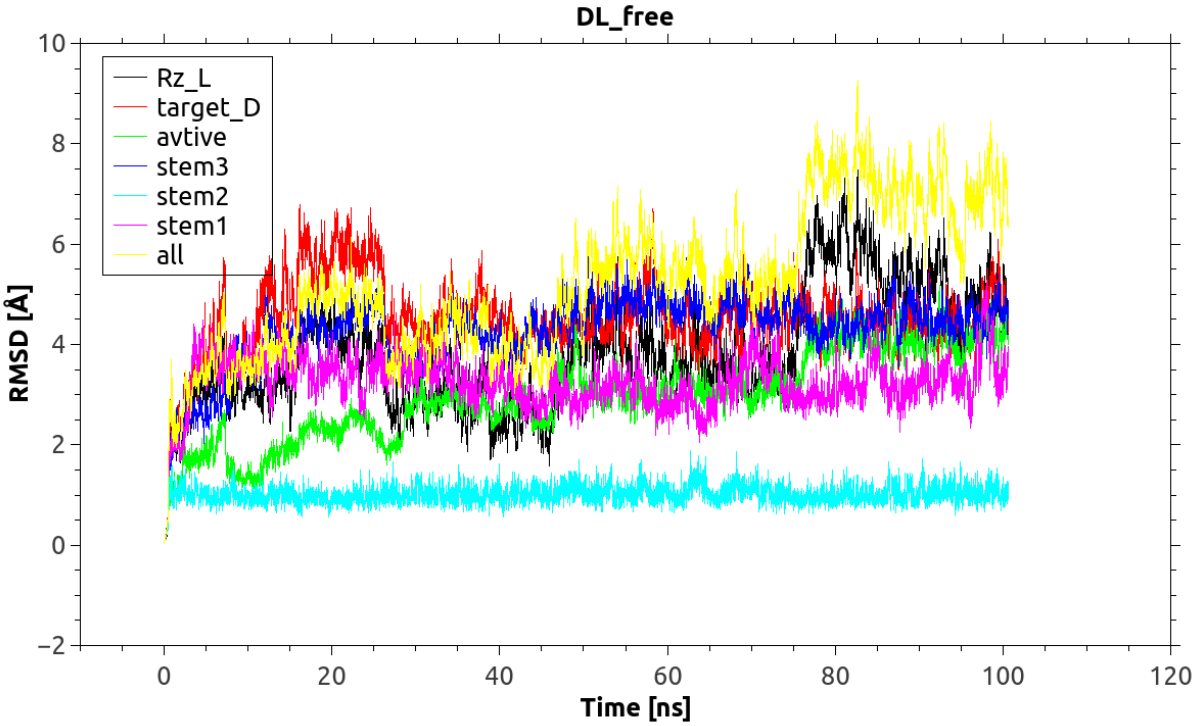
DL_free
Rz_L
target_D
avtive
stem3
stem2
stem1
all
RMSD [Å]
Time [ns]
10
8
6
4
2
0
−2
0
20
40
60
80
100
120

Supplementary Figure 8. RMSD for the whole ribozyme heterochiral complexes with substrate (LD or DL) and their structural domains calculated without any restrains.

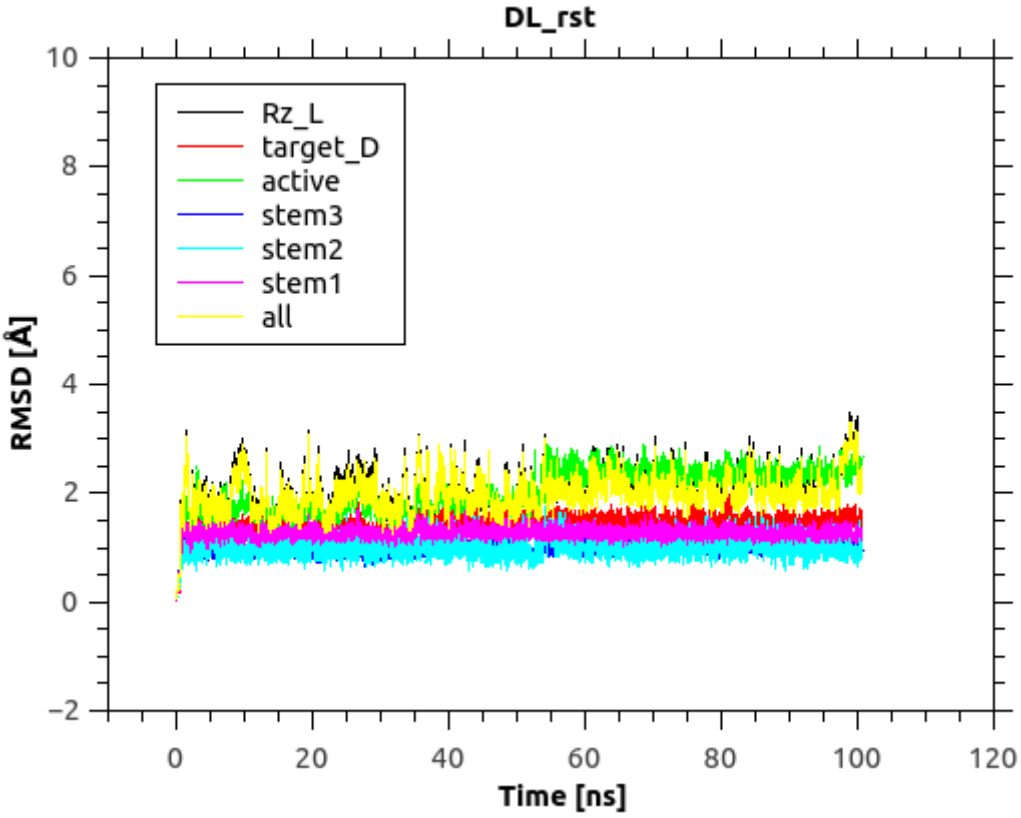
DL_rst
Rz_L
target_D
active
stem3
stem2
stem1
all
RMSD [Å]
Time [ns]
10
8
6
4
2
0
−2
0
20
40
60
80
100
120

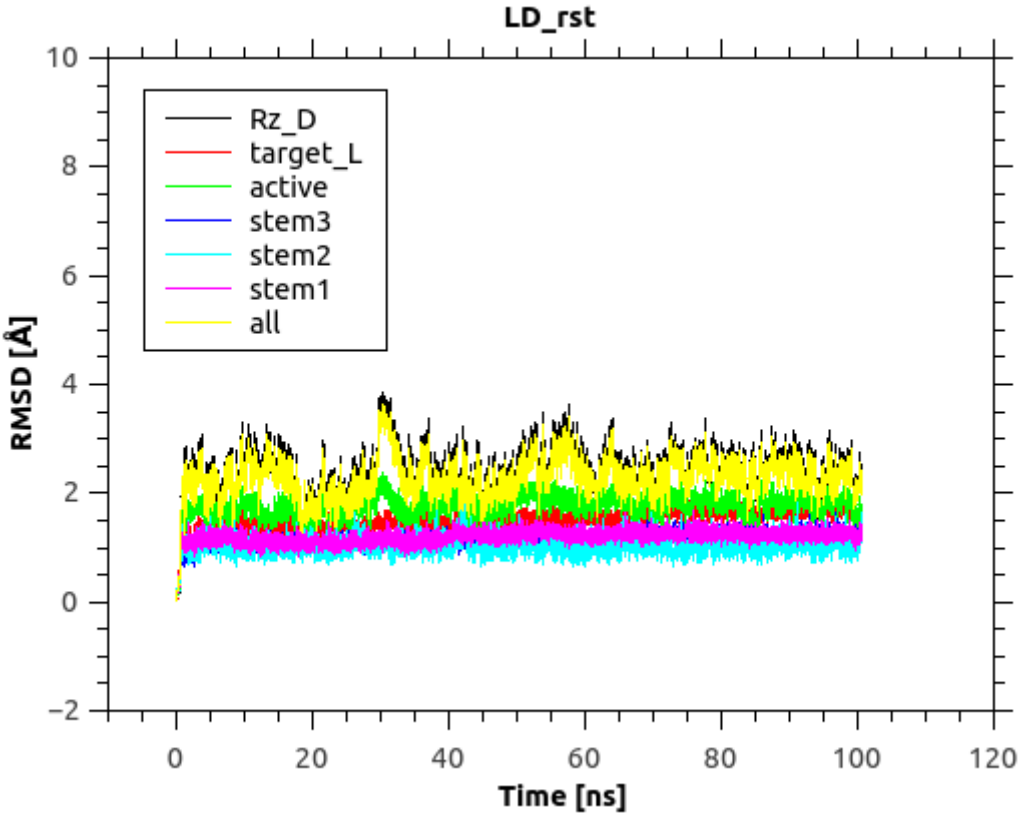
LD_rst
Rz_D
target_L
active
stem3
stem2
stem1
all
RMSD [Å]
Time [ns]
10
8
6
4
2
0
−2
0
20
40
60
80
100
120

Supplementary Figure 9. RMSD for the whole heterochiral ribozyme complex with substrate (D/L or L/D) and their structural domains calculated with positional restrains (heavy atoms).